mead Technology Laboratories

(NASA-CR-124393) COMPUTER ENHANCEMENT OF RADIOGRAPHS Final Report (Mead Technology Labs., Dayton, Ohio.) 85 p
HC $6.25 CSCL 14E

N73-31414
Unclas
G3/14 15472

Final report

Computer enhancement of radiographs

MFR-73-3

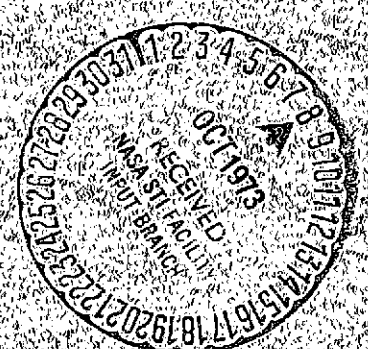

Computer enhancement of radiographs

Final report MFR-73-3
July 15, 1973
Contract No. NAS8-28521
DCN 1-2-70-00122(1F)

by
A. Dekaney
J. Keane
J. Desautels

prepared by
Mead Technology Laboratories
3481 Dayton-Xenia Road
Dayton, Ohio 45432

prepared for
George C. Marshall Space Flight Center
Marshall Space Flight Center, Alabama

This report was prepared by Mead Technology Laboratories under contract NAS8-28521 entitled "Computer Enhancement of Radiographs" for the George C. Marshall Space Flight Center of the National Aeronautics and Space Administration.

TABLE OF CONTENTS

TABLE OF CONTENTS

(Con't)

TABLE OF FIGURES

TABLES

ACKNOWLEDGEMENTS

Mead Technology Laboratories acknowledges the cooperation of Mr. Jim Holloway, Metals and Ceramics Division, NDT and Mechanics Branch (LLN), Air Force Material Laboratory, Wright-Patterson Air Force Base, Dayton, Ohio for his assistance in generating low energy x-ray radiographs and for the use of AFML's x-ray equipment.

ABSTRACT

Examination of three relevant noise processes and the image degradation associated with Marshall Space Flight Center's (MSFC) x-ray/scanning system was conducted for application to computer enhancement of radiographs using MSFC's digital filtering techniques. Graininess of type M, R single coat and R double coat x-ray films was quantified as a function of density level using root-mean-square (RMS) granularity. Quantum mottle (including film grain) was quantified as a function of the above film types, exposure level, specimen material and thickness, and film density using RMS granularity and power spectral density (PSD). For various neutral-density levels the scanning device used in digital conversion of radiographs was examined for noise characteristics which were quantified by RMS granularity and PSD. Image degradation of the entire pre-enhancement system (MG-150 x-ray device; film; and Optronics scanner) was measured using edge targets to generate Modulation Transfer Functions (MTF). The four parameters were examined as a function of scanning aperture sizes of approximately 12.5 μm, 25 μm and 50 μm.

SECTION I

INTRODUCTION

A. SETTING

X-ray generated radiography provides a valuable nondestructive method for determining the soundness of welds. X-ray radiography is widely used for the detection of discontinuities such as cracks, porosity, slag inclusions, incomplete fusion, and incomplete penetration, mainly because it offers a rapid and sensitive approach.

The mere presence of defects or flaws in a weld does not generally mean that the specimen cannot serve its intended purpose. An individual who interprets the radiograph must exercise some judgement as to the degree of imperfection that exists and must determine whether the flaw would prevent the specimen from being used. Accurate quantification of the degree of imperfection or discontinuity, therefore, demands optimum information extraction from x-ray imagery. To this end, the National Aeronautical and Space Administration (NASA) at Marshall Space Flight Center (MSFC) is engaged in digital image enhancement of weld flaws through the application of digital filtering techniques to radiographic imagery scanned on a high-speed microdensitometer.

B. PROBLEM ADDRESSED

MSFC's mode of processing the imagery is to take an x-ray generated radiograph of the weld where the flaw occurred; scan the radiograph on a high speed microdensitometer and digitize the image; enhance the digital image by the computer; then recreate the enhanced image on film. MSFC has recognized that this approach to image enhancement is constrained by the sources in the x-ray/scanning system where noise processes and other degradations can be introduced.

The tasks undertaken in this program were the specification and quantification of several of those source parameters which should be considered in the development of digital filters applicable to radiographic images processed through MSFC's system. The investigation was limited to the x-ray/scanning phases of the processing system, since the film writing phase is dependent upon the particular filtering techniques developed by MSFC. The success of the filtering process is dependent on the nature of the system preceding it and should not be constrained by the device displaying the enhanced imagery.

This study examined the relevant noise processes and image degradation inherent in the system. The noise sources considered in the program were film grain, quantum mottle and scanner noise. Film grain was examined with a fixed exposure(keV)level but with varying film type and exposure time. Quantum mottle was examined with varying exposure levels, varying film types, varying specimen material and thickness, and varying film density levels. Scanner noise was examined under varying neutral-density filter levels. These sources were

quantified through the computation of the root-mean-square (RMS) granularity, which equals the standard deviation of the noise process multiplied by 1000, and the power spectral density (PSD) function, which shows how the statistical variance of the noise process is distributed in frequency space.

The degradation considered in the program was the composite degradation introduced by the x-ray equipment, the film and the scanning device. The degradation was examined as a function of film type, exposure level, exposure time, film density and format position. Image degradation was measured by computation of the Modulation Transfer Function (MTF), which measures the degradation to a sine wave introduced by the system. The MTF can also be thought of as the Fourier transform of the point spread function of the system.

C. IMPLICATIONS

The design of digital enhancement filters depends on the system's MTF and noise characteristics (PSD) in the following manner. The MTF's of the system for various values of the physical aspects of the system indicate the resolution limits of the system. These resolution limits are important in the establishment of cut off frequencies for noise suppression filters. For example, in attempting to suppress noise frequencies beyond the highest image spatial frequencies, the resolution limits can be used as upper cutoff frequencies on low-pass filters.

The design of effective bandpass spatial filters requires that the spectral content of the noise be known. The computed noise process PSD's allow for the determination of whether or not significant noise bands can be removed without seriously affecting image spatial frequencies.

D. FORMAT

The remainder of this report discusses the data acquisition for examination of the relevant system parameters mentioned above, the analysis of the data and the impact of each parameter on digital filtering. All pertinent tables and figures are found in the body of the report. The details of the data analysis techniques used in this study are presented in the Appendix.

SECTION II
DATA ACQUISITION

In order to evaluate the significance of film graininess, quantum mottle, scanner noise and image degradation, test radiographs and neutral-density filters must be generated and converted to digital form. This section discusses the procedures followed to generate the radiographs and select the neutral-density filters for each of the areas listed above. It also discusses the techniques employed to convert these data to digital form.

A. FILM GRAININESS

The purpose of the film graininess portion of the program was to determine the granularity of x-ray film types R single (SC), R double (DC), and M. Proper exposure of film for this investigation required extremely low energy x-rays. Low energy x-ray exposure makes it impossible for one x-ray photon to expose more than one film grain. Insuring that each photon exposed no more than a single grain permitted the generation of radiographs free of quantum mottle. In addition, exposure with low energy x-rays permitted grain exposure throughout the depth of the emulsion as opposed to exposure with light which tends to expose grains at the surface of the emulsion.

1. Radiograph Generation: In total fourteen exposures were generated using low energy x-rays. For film type R (SC) five exposures were made at density levels of 1.04, 1.55, 1.80, 1.90, and 2.75D. The type R (DC) film was exposed to the five density levels of 1.18, 1.46, 1.60, 2.06, 2.60D. Four density levels were generated on type M film at density levels of .99, 1.46, 2.06, and 2.18D.

Radiographs used for the granularity investigation were produced on film supplied by MSFC. This film was taken from the same packages as the film used in the quantum mottle and MTF portions of this investigation which will be discussed later. The film was exposed with an 8 keV x-ray system similar to that depicted by Figure 1. As discussed above, the 8 keV x-ray source resulted in radiographs relatively free of quantum mottle. The vacuum path from the x-ray source to the film reduced the attenuation of the 8 keV x-rays. The paper cassette in which the film was packed was removed to further reduce the attenuation of the 8 keV x-rays and to eliminate noise caused by the fiberous material in the cassette paper. All exposures were made with an x-ray tube current of 10 ma. Variation in exposure levels and ultimately film density levels was obtained by varying the exposure time from .5 to 3.0 minutes.

2. Film Processing: The exposed films were processed manually using Kodak x-ray developer and Kodak fixer. Five minute development at 70^{o}F was used as described in the "Film Processing Supplement" to Radiography In Modern Industry, by Eastman Kodak Company, Rochester, New York. All processing was performed within a twenty hour period after the film was exposed, in order to minimize latent image failure.

3. Data Conversion: The developed fourteen radiographs were scanned on Mead Technology Laboratories' Mann Micro-Analyzer. Set-up procedures for

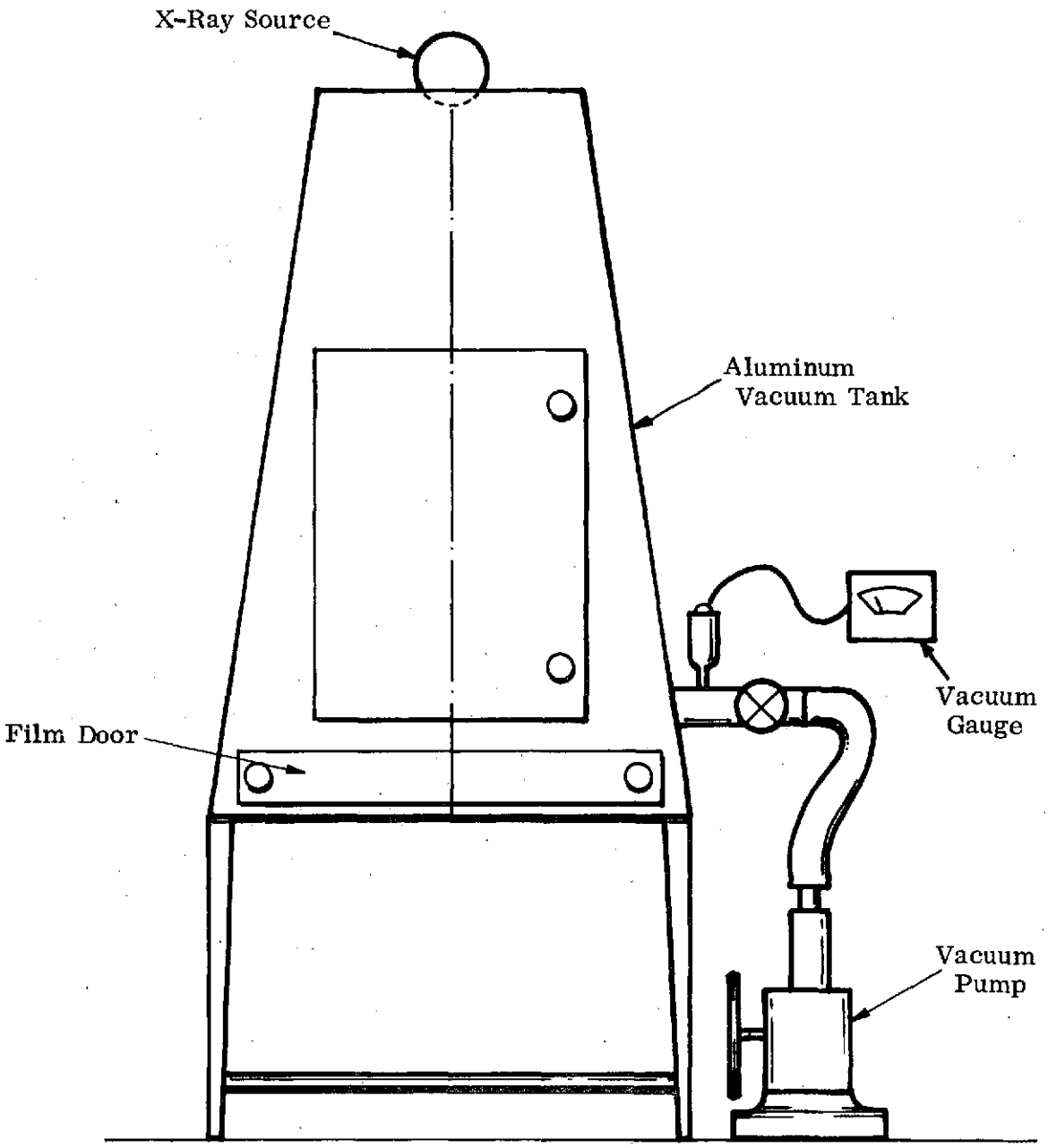

Figure 1. 8 keV X-Ray System

Micro-Analyzer scanning are discussed in Appendix I. Three circular scanning apertures (13, 27, and 57 micrometers) approximating the apertures available on MSFC's high speed scanner were used to scan the radiographs. To provide for comparison of results among the aperture settings the three radiograph scans were taken over the same area. A minimum of 6144 samples were taken in each scan. A sampling interval equal to or greater than the diameter of the aperture was used in each scan to assure that the resulting samples would be uncorrelated as required by the analysis procedures.

B. QUANTUM MOTTLE

The purpose in examining quantum mottle was to characterize it as a function of x-ray energy, specimen filter, film type, density of the radiograph, and presence or absence of intensifying screen through the computation of RMS granularity and PSD. Since the scope of each of these parameters is large, the examination of mottle was limited to specific parameter values pertinent to MSFC's inspection of weld flaws.

1. Parameter Selection: The investigation of quantum mottle was limited to five material specimens (three aluminum and two steel), three film types, lead screen and no screens, five film density levels, and three exposure levels. The following paragraphs provide a brief statement of the rationale for selecting the specific parameter values for the quantum mottle experiments.

The choice of film types M, R (DC) and R (SC) was made by mutual agreement of MSFC and Mead Technology Laboratories personnel, in order to examine films currently being used in MSFC applications and films considered for future applications. In order to determine the effects of screens on mottle and yet restrict the number of experiments to a reasonable number, the decision was made to generate a complete set of radiographs without screens, while running a few selected experiments for replication with screens.

The specimen materials were selected to be representative of those which normally are candidates for ultimate digital filtering enhancement. Therefore, aluminum and steel were chosen as the experimental specimen materials. Material thicknesses were also chosen to represent normal operations and to limit the number of experiments to a manageable number. Thus 1/4, 1/2 and 3/4 inch aluminum specimens and 1/8 and 1/4 inch steel specimens were specified for the experiments.

The majority of radiographs considered for enhancement by MSFC are exposed to an approximate density level of 1.7D. To provide for a measure of completeness in this investigation, the density range under consideration was made to vary from this nominal by approximately $\pm$ .8D. Also, to maintain a manageable number of experiments, the specific number of densities investigated was limited to five levels. These levels were approximately 1.0, 1.3, 1.7, 2.0, and 2.5D.

The energy level normally used by MSFC for weld flaw inspection lies in a neighborhood of 100 keV. Thus, to make the experiments meaningful and also relatively complete, five energy levels (30, 50, 100, 200, and 300 keV) were initially selected for the investigation. However, performance of the

experiment indicated that the two lowest x-ray energies (30, 50) were impractical due to the extended exposure period required and subsequently were deleted from consideration. 1/4 inch steel was selected for replication with screen at the 200 keV energy level, simulating operational procedures. The complete set of radiographs generated for the quantum mottle examination are described in Table 1 below.

KEV	MATERIAL		DENSITY				
	Type	in.	1.0	1.3	1.7	2.0	2.5
100	Alum.	1/4	1,2	1,2	1,2	1,2	1,2
		1/2	1,2	1,2	1,2	1,2	1,2
		3/4	1,2	1,2	1,2	1,2	1,2
	Steel	1/8					
		1/4	2,3	2,3	2,3	2,3	2,3
200	Steel	1/8					
		1/4	1,2,3	1,2,3	1,2,3	1,2,3	1,2,3
300	Steel	1/8	2,3	2,3	2,3	2,3	2,3
		1/4					

Table 1. Quantum Mottle Exposures

2. Exposure Procedures: The radiographs for the quantum mottle examination were exposed at the MSFC nondestructive testing laboratory. The focal spot of MSFC's MG-150 x-ray unit was positioned 80 inches above the floor with the x-ray beam pointing toward the floor. The holder for the film cassette was mounted to support the film 40 inches from the focal spot. The floor was covered with a lead sheet at least 1/8 inch thick over the x-ray beam area.

The cassette support was made in the form of a frame to provide support at the edges of the cassette and to avoid backscatter. The cassette was covered with a lead mask 1/4 inch thick which was cut 1/4 inch smaller in the inside dimensions than the support frame. The sizing prevented backscatter from the frame at the edges. The experimental configuration of the x-ray equipment is shown in Figure 2.

For this particular task, the specimen was to act as a filter in absorbing the soft radiation without creating an image. Hence, the specimen was located as close to the x-ray target as possible but was not placed directly on the cassette as in normal radiographs. Placement of the material close to the focal spot caused hidden manufacturing flaws present in the material to be spread across the film format in a manner similar to effect of geometric unsharpness. Therefore, contributions of such anomalies to the mottle and grain noise were minimized.

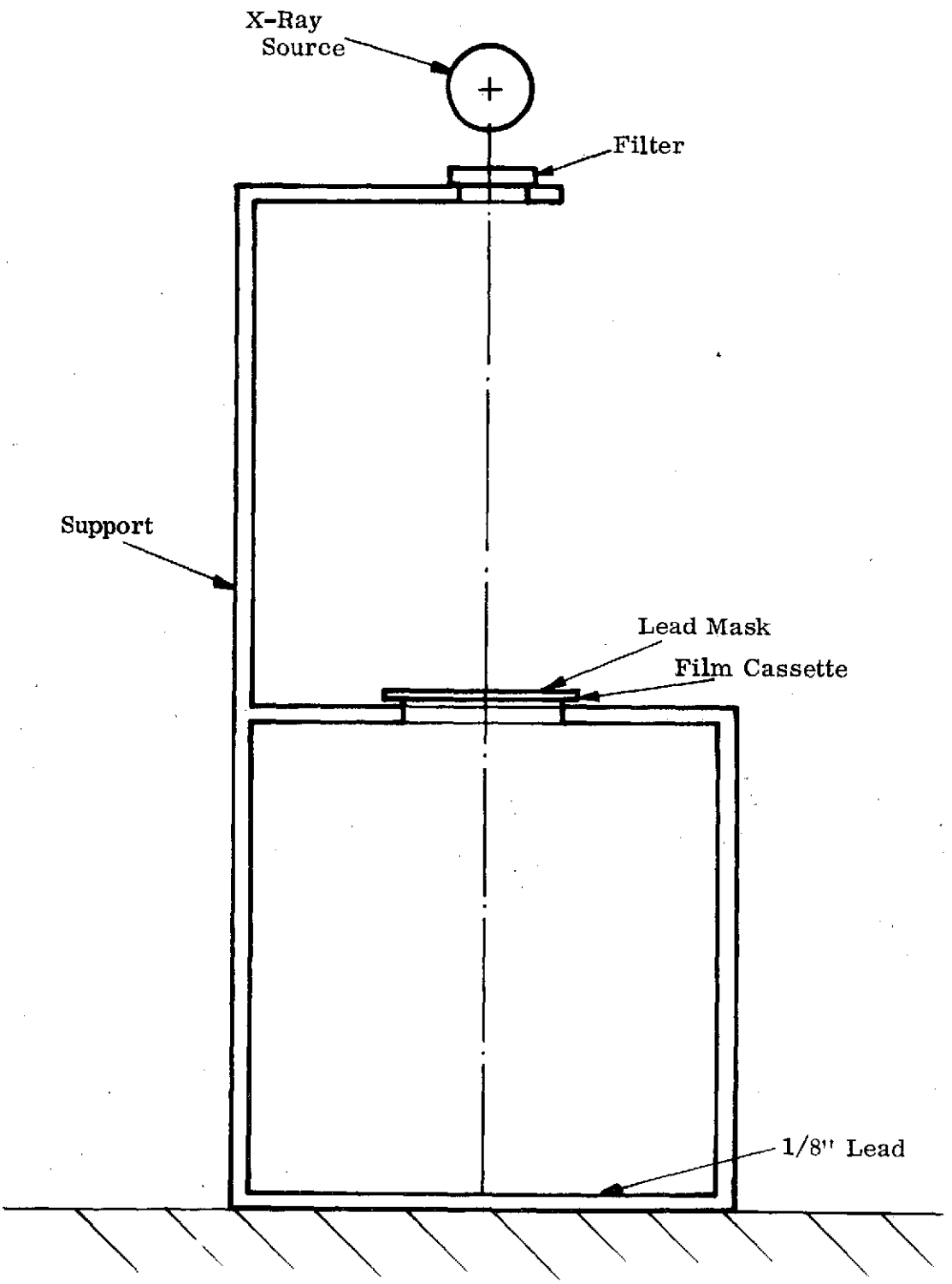

Figure 2. MG-150 Experimental Configuration

3. Film Processing: To maintain maximum processing control and to minimize latent image failure, all radiographs were manually processed within twenty-four hours of exposure at MSFC. The processing conditions employed were 4.5 minutes in 70^{o} developer, followed by a 30 second stopbath and 15 minutes in a fixing solution. The radiographs were washed and then treated with photo flow to prevent water spotting. The finished radiographs were forwarded to Mead Technology Laboratories for analysis.

4. Data Conversion: The techniques employed to reduce the radiographs for the quantum mottle examination to digital form were identical to those techniques employed for the film granularity experiment. (See Section II, A.3) The same Micro-Analyzer parameters were employed to analyze these radiographs. Several of the radiographs were not scanned with all three Micro-Analyzer spots. The reason for their omission was that analysis of initial scan data indicated new information would not be obtained from these additional scans.

To more meaningfully relate the quantum mottle investigation to MSFC's image processing facility, several radiographs were selected for scanning with MSFC's Optronics scanner. These film specimens were scanned with 12.5 μm, 25 μm, and 50 μm apertures using equivalent sampling intervals. The density mode selector was set to 0-3D range.

C. SCANNER NOISE

MSFC's Optronics scanner represents a potential noise source in the digital filtering system. The purpose of examining this element of the system is to identify the variance and spectrum of the noise process associated with the scanner and to examine them for their influence on the filtering process.

1. Neutral-Density Filter Specification: The noise characteristics of the drum type scanner were determined by scanning, digitizing, and analyzing several Kodak neutral-density filters. Neutral-density filters were selected as targets since they represent uniform density patches with minimum inherent noise. Ten filters were used to represent the density range .18 to 2.39D. The specific density values of the filters were .18, .48, .82, .98, 1.16, 1.50, 1.76, 1.94, 2.19, and 2.39D. It is not necessary to scan the entire specimen to obtain a sufficient sample size, hence a 1 cm. wide rectangular area served as the noise target.

2. Data Collection: The filters were prepunched and mounted in the upper left hand corner of the drum. The top of the filter was supported by and clamped to the drum, whereas the left edge was supported by and taped to the drum. Support was believed sufficient to allow the filters to assume the curved contour of the drum.

Scanning was accomplished under the following parameterization:

- 0-3D Density Range
- Start of record set at 2
- End of record set at 6
- Left X selector set at 3
- Right X selector set at 4

Each of the ten filters was scanned under the above conditions repeated with apertures and sampling intervals of 12.5 μm, 25 μm, and 50 μm.

D. IMAGE DEGRADATION

The purpose of investigating image degradation was to provide MTF data which could be utilized in selecting digital filters for application to enhancement of radiographs. The method selected to obtain this information was the analysis of edge targets which consist of two distinct uniformly thick specimens whose boundary is a plane. By producing radiographs containing edges, scanning the radiographs with the Optronics scanner and analyzing the resulting digital data, the MTF for the entire x-ray scanning system (including x-ray source, film, processing and scanner) was computed.

In the design of the experiment to compute the MTF, several parameters which could affect the MTF of the system were considered for investigation. The parameters selected were film type, density difference per edge, average density per edge target, x-ray energy level, and distance from the center of format. These parameters were selected because they were likely to significantly influence the system MTF and because they would normally be variables in actual applications.

1. Target Development: Generation of radiographs for edge analysis required the design and manufacturing of two targets. The wedge target shown in Figure 3 was designed to provide twelve density levels which formed eleven edges of approximately equal density difference. The purposes of the wedge target were to provide an overall check on the x-ray system linearity and, if possible, to become a source of low modulation edges. The edge target shown in Figure 4 was designed to provide seven edges of varying density differences with approximately the same mean density. Both the wedge and edge targets were machined out of 2419 aluminum.

Since lower modulation flaws would be of primary interest in practice, the targets had to be exposed in such a way to assure that edges of minimum analyzable density amplitude would be available. The thickness differences existing in the targets were designed so that the density difference recorded on the radiographs would range from 0.04 to 0.50D. This range of density differences would provide an input signal for the scanner ranging from less than the scanner's minimum detectable density difference to ten times the minimum detectable density difference.

2. Radiograph Generation: Identical geometry was used to expose all nine radiographs for the MTF investigation. The two targets described earlier were placed in direct contact with the paper film cassettes at the center of the film format. The film and targets were placed on a lead covered table with the focal spot of the x-ray tube 40 inches above the center of the film. This particular geometric configuration was selected because it simulated actual radiographic conditions encountered at the MSFC nondestructive test facility. Variation in image density was achieved through a combination of varied exposure time, varied x-ray tube current and insertion of filter material under the target. The various exposure conditions are listed in Table 2.

NOTE: MATERIAL — 2219 Al
View "A" All Dimensions ± 0.05
View "B" All Dimensions ± 0.002

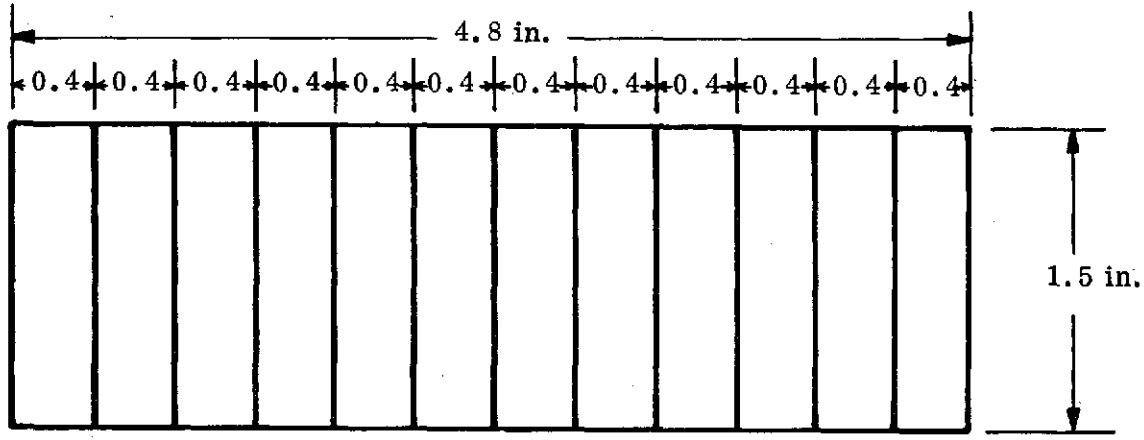

VIEW "A"

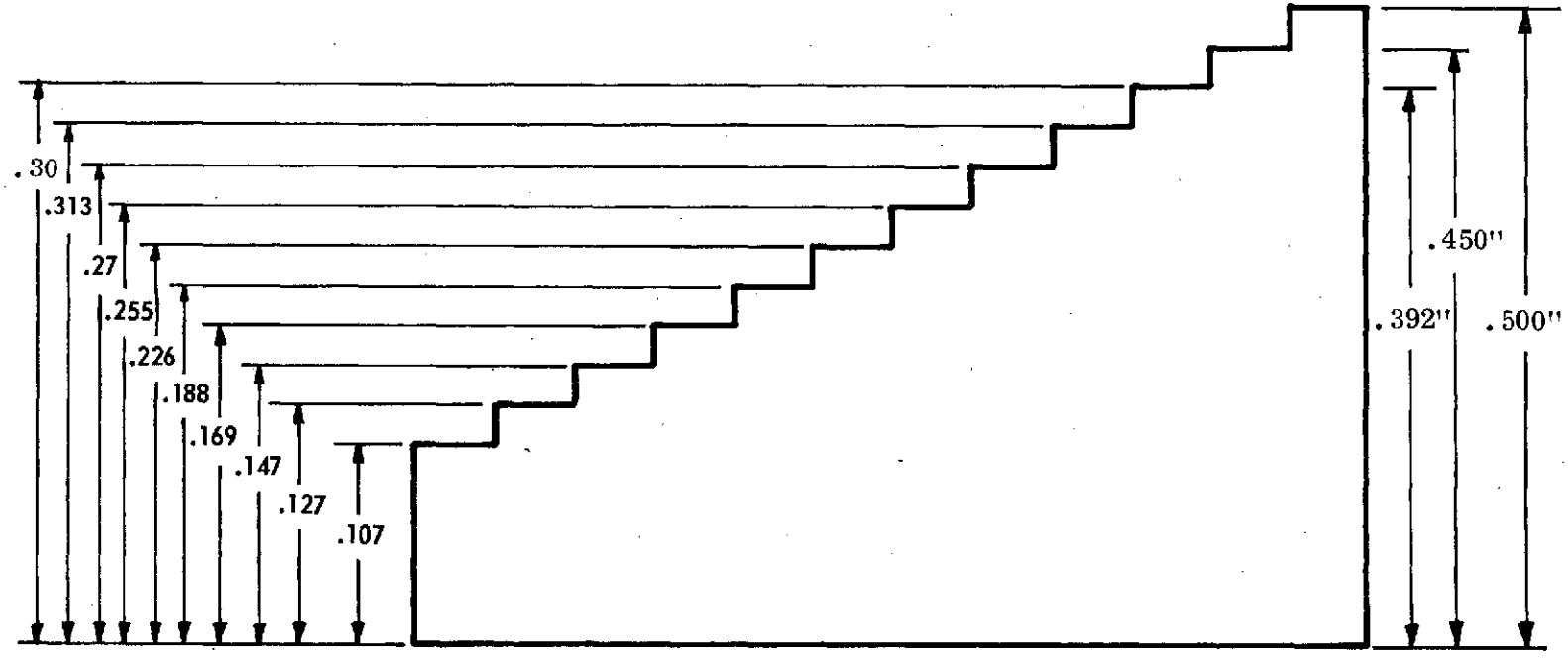

VIEW "B"

Figure 3. Wedge Target

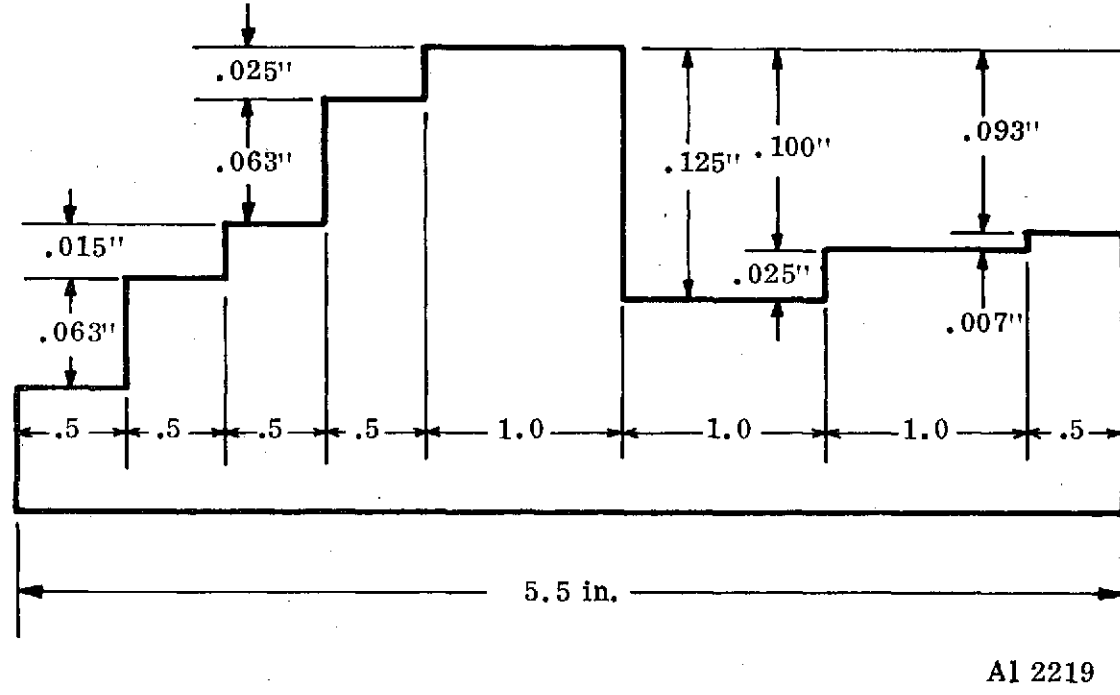

Figure 4. Edge Target

Radiograph Identification	keV Level	Film Type	Exposure Time
100-2-2.5	100	R (DC)	2.5 min.
70-3-2	70	M	2.0 min.
200-1-1	200	R (SC)	1.0 min.
100-1-4.2	100	R (SC)	4.2 min.
100-3-1	100	M	1.0 min.
200-1-1.5	200	R (SC)	1.5 min.
80-3-2	80	M	2 min.
100-1-4	100	R (SC)	4 min.
100-3-1.5	100	M	1.5 min.

Table 2. Exposure Conditions for Edge Analysis Radiographs

The radiographs were processed at MSFC immediately following exposure under the same conditions as those employed for the quantum mottle radiographs. Each step on the radiographs was subsequently read by a MacBeth densitometer. The values of the readings are found in Table 3.

3. Data Reduction: The nine radiographs were digitized on MSFC's Optronics scanning device in such a manner that the direction of scan was nearly perpendicular to the edges on the film. At least one hundred scan lines were taken across each edge in three locations (at approximately the center and at the two extremities). The scanning was performed in a 0-3D density mode using the 12.5 μm sampling and aperture settings, with the data recorded on magnetic tape for subsequent computer analysis. The length of each scan was constrained so that a sufficient number of samples would be taken to include the entire edge response.

Exposure Conditions Identification	Step Number 1	2	3	4	5	6	7	8	9	10	11	12
100-2-2.5 min.	.95 1.85	1.04 1.94	1.19 2.08	1.42 1.55	1.51 1.63	1.61 1.88	1.72 1.93	1.84 2.22	1.97	2.07	2.16	2.28
70-3-2 min.	.74 1.01	.87 1.04	1.08 1.16	1.51 .76	1.70 .82	1.95 1.01	2.22 1.07	2.54 1.36	3.02	3.43	3.86	4.40
200-1-1 min.	.88 1.54	.94 1.42	1.02 1.50	1.15 1.22	1.21 1.27	1.26 1.40	1.32 1.43	1.38 1.57	1.45	1.50	1.54	1.57
100-1-4.2 min.	1.06 1.53	1.17 1.57	1.32 1.67	1.56 1.29	1.66 1.36	1.81 1.55	1.94 1.60	2.08 1.84	2.25	2.39	2.52	2.67
100-3-1 min.	.78 1.27	.89 1.32	1.00 1.42	1.21 1.05	1.31 1.11	1.41 1.30	1.53 1.36	1.65 1.58	1.80	1.93	2.05	2.17
200-1-1.5 min.	1.24 1.95	1.35 2.07	1.46 2.18	1.65 1.75	1.73 1.82	1.83 2.01	1.93 2.05	1.99 2.25	2.08	2.17	2.22	2.27
80-3-2 min.	1.26 1.70	1.50 1.74	1.81 1.92	2.41 1.31	2.71 1.42	3.10 1.73	3.52 1.82	3.98 2.23	4.40			
100-1-4 min.	.99 1.90	1.08 1.99	1.22 2.17	1.44 1.57	1.54 1.65	1.64 1.92	1.77 1.98	1.88 2.28	2.04	2.14	2.24	.236
100-3-1.5 min.	.93 1.85	1.04 1.93	1.18 2.08	1.40 1.54	1.50 1.63	1.62 1.90	1.75 1.99	1.87 2.31	2.04	2.16	2.26	2.36

Table Entries are MacBeth Density Reading of Each Step in the Wedge (First entry in box) and Edge (Second entry in the box)

x-y-z, where x = keV Level
y = Film Type (1 = R (SC), 2 = R (DC), 3 = M)
z = Exposure Time

Table 3. Density Levels of Edges

SECTION III

DATA ANALYSIS

A. FILM GRANULARITY

The digital data obtained from the Micro-Analyzer scans of the 8 keV generated radiographs was analyzed by computing the RMS granularity for the fourteen film specimens. A complete description of RMS granularity theory and computational technique is presented in Appendix II. The examination of the film granularity as a function of film type, density level and scanning aperture is summarized by the RMS granularity numbers presented in Tables 4, 5, and 6.

Careful examination of the granularity data contained in these tables indicates that the resulting granularity does not show smooth or uniform trends. The erratic nature of the data, in large measure, can be attributed to difficulities encountered in the course of the experiment. These difficulties included the fact that the x-ray system used to expose the radiographs was not ideally suited for the performance of low noise experiments, since it was operating at an energy level below its normal operating range and some scattering resulted from the metal walls of the vacuum chamber. Also, the experiments were conducted over an extended period of time resulting in difficulty maintaining control of the processing chemistry.

One would normally expect to see two trends in the data presented in Tables 4, 5, and 6. As the density level increases for a fixed film and aperture size, the granularity level should increase [1], and for a fixed film type and density level the granularity should decrease as the aperture size increases [2]. The latter of these trends occurs in the granularity data while the former does not strictly occur (for the reasons discussed above).

---

1 Herz, R. H., The Photographic Action of Ionizing Radiations, Wiley-Interscience, New York, 1969, pp 140-141.

2 This is due to the smoothing effects resulting from wider spread functions of larger apertures.

Film Density	Aperture Diameter		
	Micro-Analyzer		
	13μ	27μ	57μ
1. 1.04	24	19.0	11.3
2. 1.55	38	32.0	14.5
3. 1.80	33	28.0	14.3
4. 1.90	31.6		14.5
5. 2.75	29.3	22.0	12.3

Table 4. RMS Granularity R (SC), 8 keV

Film Density	Aperture Diameter		
	Micro-Analyzer		
	13μ	27μ	57μ
1. 1.18	25	25.3	14
2. 1.46	26.6	20.6	12.0
3. 1.60	29.0	23	13.0
4. 2.06	33.0	24	14.6
5. 2.60	35	26	14.0

Table 5. RMS Granularity R (DC), 8 keV

Film Density	Aperture Diameter		
	Micro-Analyzer		
	13μ	27μ	57μ
1. .99	26.6	19.3	11.0
2. 1.46	29.3	22.0	12.6
3. 2.06	37.0	25.3	13.0
4. 2.18	30.3	24.3	13.3

Table 6. RMS Granularity M, 8 keV

B. QUANTUM MOTTLE

1. RMS Granularity: The sixty-five radiographs generated in this phase of the program were analyzed under varying scanning aperture conditions. All were analyzed for RMS granularity with 27 μm and 57 μm aperture scans using the Micro-Analyzer and most were analyzed using a 13 μm aperture. As was previously noted several of the radiographs were digitized on the Optronics scanner using the 12.5 μm, 25 μm, and 50 μm scanning apertures. The RMS granularity for the Micro-Analyzer generated data is seen in Tables 7 through 20. When appropriate the associated RMS granularity values as computed from the Optronics scanner are included.

The number preceding the slash in the Optronics sections of Tables 7 through 20 is one thousand times the standard deviation of the digital values read from the Optronics scanner. The number following the slash is the digital standard deviation multiplied by a constant and relates the standard deviation to an effective RMS granularity value. The constant is one thousand times the slope of the effective calibration curve. The effective calibration of the Optronics scanner for x-ray's is illustrated by the curve in Figure 5.

To more readily demonstrate the findings of the quantum mottle investigation data selected from Tables 7 through 20 have been presented graphically in Figures 6 through 14. In Figure 6 the effect of scanner aperture size and image density is demonstrated for type R (SC) film. As was expected the measured film granularity increased with decreasing spot size. For photographic films this increase in granularity with decreasing aperture size follows Selwyns Law. For x-ray film Selwyn's Law is known not to hold. This figure also demonstrates that for all three apertures there is a nearly linear increase in granularity with increasing density over the density range from 1.0 to 2.0 and that the granularity takes a slight drop at densities in excess of 2.0.

In Figures 7 and 8 results similar to those found for R (SC) are demonstrated for type R (DC) and type M film. Both films show an increase in granularity with a decrease in aperture size. For all three apertures with both films there is again a nearly linear increase in granularity with increasing density over the 1.0 to 2.0 density range followed by a drop in granularity for densities greater than 2.2.

Figure 9 demonstrates the relationship among the granularities measured for the three film types with the 13 micrometer spot. Type R (DC) demonstrates the lowest granularity over the entire density range investigated. Type R (SC) film demonstrates a substantially higher granularity than R (DC) over the density range. Since both R-type films are made with the same emulsion, the difference in granularity measured for the two films is interesting to say the least. The different granularity for the two films is most likely the result of the difference in the arrangement of the emulsion layers. Because of the complexity the situation where the scan aperture interogates emulsion layers separated by a distance several times greater than the diameter of aperture, no model has been developed to explain the difference between the R type film in the granularity measurements.

Film Density	Aperture Diameter					
	Micro-Analyzer			Optronics		
	13 μ	27 μ	57 μ	12.5 μ	25 μ	50 μ
1. 1.10	49.0	33.6	21.0	11/39.6	8/28.8	5.0/18
2. 1.30	53.0	36.3	21.3	12/43.2	9/32.4	6.0/21.6
3. 1.69	58.0	42.3	26.0	11/39.6	10/36.0	6.5/23.4
4. 1.95	61.0	44.3	29.0		11/39/6	7.0/25.2
5. 2.35	56.0	41.3	25.0			

Table 7. RMS Granularity M, 100 keV, Fe (.25 inch)

Film Density	Aperture Diameter					
	Micro-Analyzer			Optronics		
	13 μ	27 μ	57 μ	12.5 μ	25 μ	50 μ
1. 1.03	46.3	34.6	21.0		6.5/2.34	7/25.2
2. 1.39	61	44	27.2		4/14.4	4/14.4
3. 1.70	65.0	46.6	29.7	8/28.8	8/28.8	6.0/21.6
4. 2.02	66.3	48	29.7		4.0/14.4	4.2/15.1
5. 2.58	48	36.6	22.0			

Table 8. RMS Granularity M, 200 keV, Fe (.25 inch)

Film Density	Aperture Diameter					
	Micro-Analyzer			Optronics		
	13 μ	27 μ	57 μ	12.5 μ	25 μ	50 μ
1. 0.98	46.6	33.0	20.4	4/14.4	4/14.4	4/14.4
2. 1.35	56.3	39.3	25.7	12/43.2	10/36.0	6.5/23.4
3. 1.81	59.0	40.6	27.4	11/38.6	11/39.6	7/25.2
4. 2.18	64.0	46.0	28.8	7/25.2	10.5/37.8	6/21.6
5. 2.36	62.0	43.0	27.7			

Table 9. RMS Granularity M, 300 keV, Fe (.125 inch)

Film Density	Aperture Diameter		
	Micro-Analyzer		
	13μ	27μ	57μ
1. 0.90	45.6	32.0	20.3
2. 1.56	58.6	43.3	26.3
3. 2.39	61.0	45.0	28.0
4. 2.93	35.0	26.3	15.6

Table 10. RMS Granularity M (with screens), 200 keV, Fe (.25 inch)

Film Density	Aperture Diameter	
	Micro-Analyzer	
	27μ	57μ
1. 1.04	31.3	19.0
2. 1.45	41.0	23.0
3. 1.68	46.6	27.0
4. 2.08	56.3	33.0
5. 2.61	44.3	29.0

Table 11. RMS Granularity R (SC), 100 keV, Al (.25 inch)

Film Density	Aperture Diameter					
	Micro-Analyzer			Optronics		
	13μ	27μ	57μ	12.5μ	25μ	50μ
1. 1.00	40.3	33.0	19.0			
2. 1.30	48.0	41.3	22.0	15.1/54.3	10.4/37.4	6.0/21.6
3. 1.79	63.0	52.0	30.6	13.6/48.9	12.1/43.5	14.1/50.4
4. 1.99	67.0	57.3	33	14.2/51.1	14.2/51.1	8/28.8
5. 2.66	63.0	53.0	30.6			

Table 12. RMS Granularity R (SC), 100 keV, Al (.50 inch)

Film Density	Aperture Diameter	
	Micro-Analyzer	
	27μ	57μ
1. 1.11	31.3	19.6
2. 1.31	39.6	24.3
3. 1.63	45.6	27.0
4. 2.10	58.0	40
5. 2.59	48.0	30

Table 13. RMS Granularity R (SC), 100 keV, Al (.73 inch)

Film Density	Aperture Diameter		
	Micro-Analyzer		
	13μ	27μ	57μ
1. .97	38.0	33.0	19.7
2. 1.30	45.0	39.3	21.5
3. 1.77	58.0	52.6	29.3
4. 1.91	58.0	54.0	30.6
5. 2.30	65.0	59.0	33.1

Table 14. RMS Granularity R (SC), 200 keV, Al (.25 inch)

Film Density	Aperture Diameter	
	Micro-Analyzer	
	27μ	57μ
1. 1.00	24.6	15.0
2. 1.41	29.3	16.6
3. 1.60	30.6	17.0
4. 1.95	31.6	20.6
5. 2.64	26.7	17.0

Table 15. RMS Granularity R (DC), 100 keV, Al (.25 inch)

Film Density	Aperture Diameter		
	Micro-Analyzer		
	13μ	27μ	57μ
1. .99	35.6	23.0	14.6
2. 1.31	41.0	26.6	16.6
3. 1.67	46.0	28.6	17.6
4. 2.12	47.6	30	20
5. 2.41	46.6	29.0	19

Table 16. RMS Granularity R (DC), 100 keV, Al (.50 inch)

Film Density	Aperture Diameter	
	Micro-Analyzer	
	27μ	57μ
1. .94	25.6	14.0
2. 1.38	31.0	18.0
3. 1.74	33.0	18.0
4. 1.94	34	22.0
5. 2.42	29.6	19.0

Table 17. RMS Granularity R (DC), 100 keV, Al (.75 inch)

Film Density	Aperture Diameter					
	Micro-Analyzer			Optronics		
	13μ	27μ	57μ	12.5μ	25μ	50μ
1. .94		22.3	12.3	6/21.6	5/18.0	4/14.4
2. 1.27		26.6	14.6	9/32.4	7/25.2	5.0/18.0
3. 1.60		29.6	16.6	6/21.6	5.0/18.0	4/14.4
4. 1.97		31.3	17.0		8/28.8	
5. 2.31		27.6	19.0			

Table 18. RMS Granularity R (DC), 100 keV, Fe (.25 inch)

Film Density	Aperture Diameter		
	Micro-Analyzer		
	13μ	27μ	57μ
1. 1.07	35.6	24.6	15.9
2. 1.39	41.3	29	18.0
3. 1.72	44.3	32	19.2
4. 2.21	46.3	31.6	20.1
5. 2.45	44.0	33.0	18.3

Table 19. RMS Granularity R (DC), 200 keV, Fe (.25 inch)

Film Density	Aperture Diameter		
	Micro-Analyzer		
	13μ	27μ	57μ
1. 1.00	35.0	25.0	14.7
2. 1.40	43.6	30.3	19.7
3. 1.77	46.2	32.3	20.3
4. 2.14	47.6	33.6	20.1
5. 2.48	45.0	31.6	17.7

Table 20. RMS Granularity R (DC), 300 keV, Fe (.125 inch)

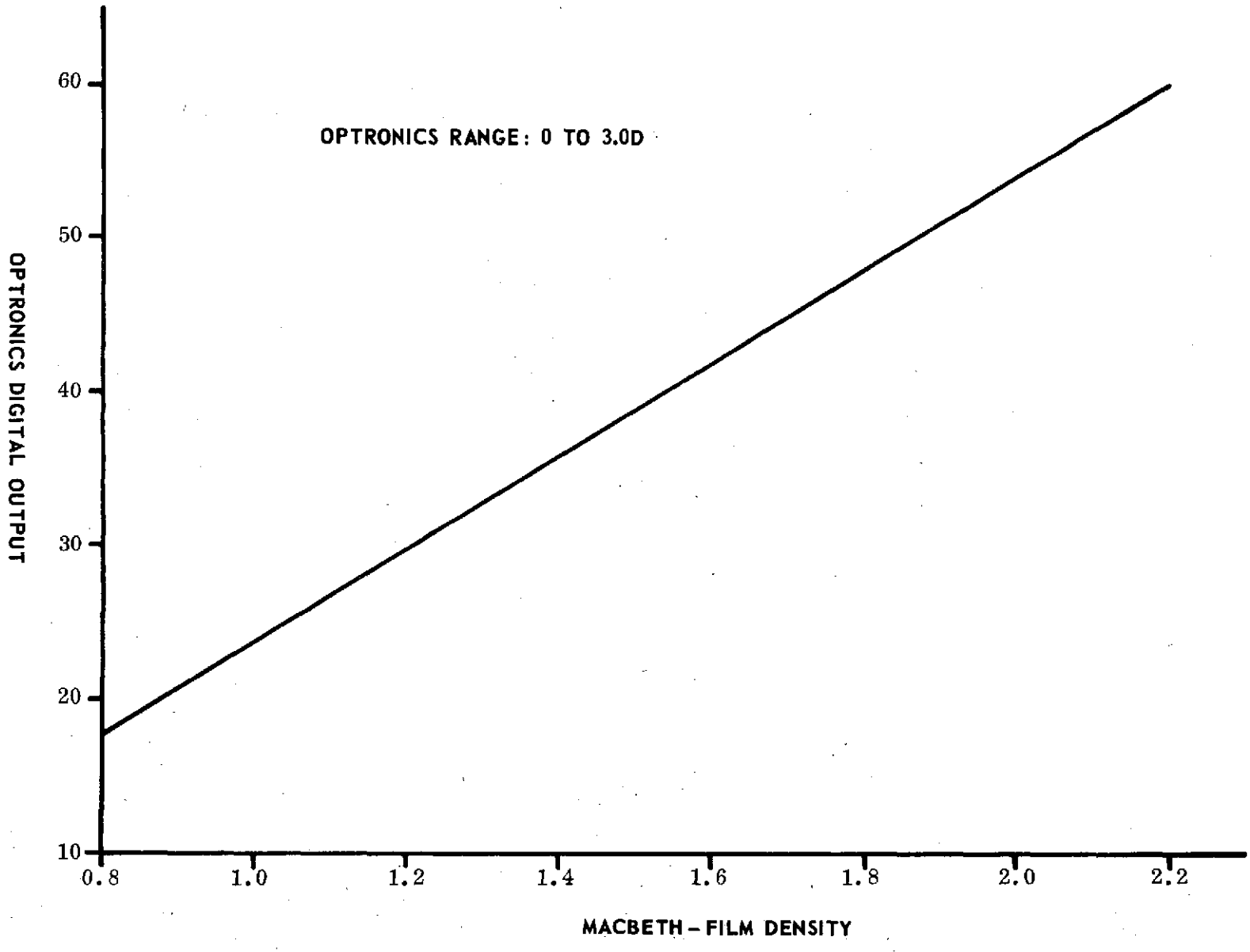

Figure 5. Effective Calibration of MSFC's Scanner

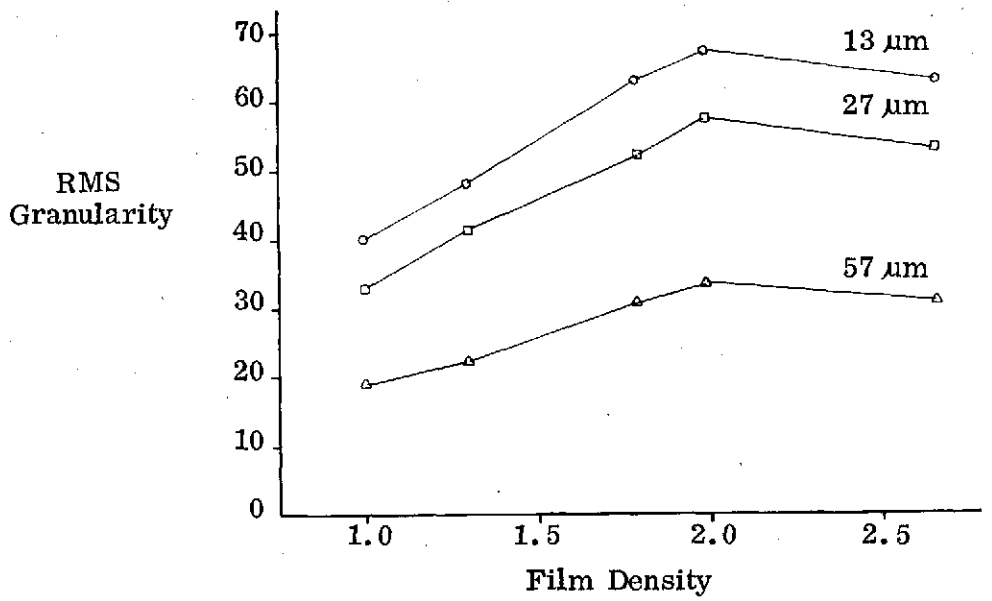

Figure 6. Comparison of RMS Granularity by Aperture for R (SC)
100 keV, Al (.50 inch)

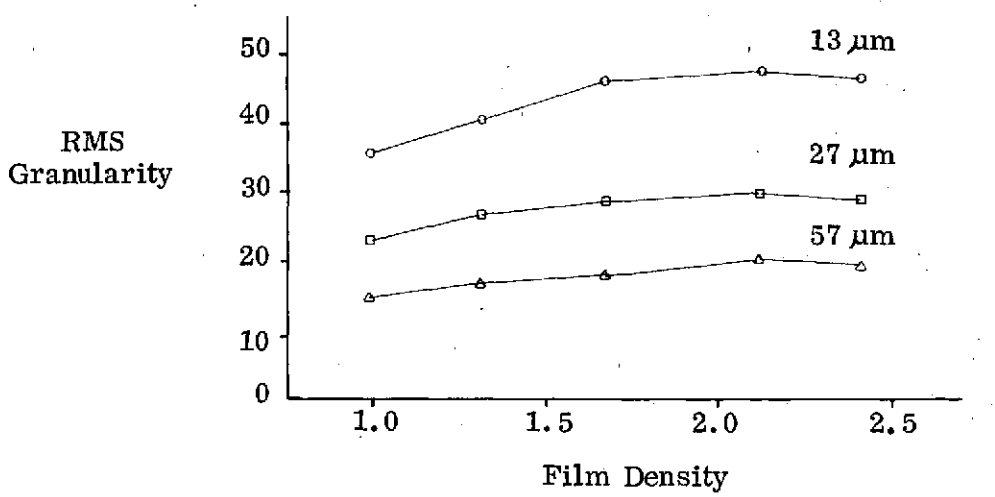

Figure 7. Comparison of RMS Granularity by Aperture for R (DC)
200 keV, Al (.50 inch)

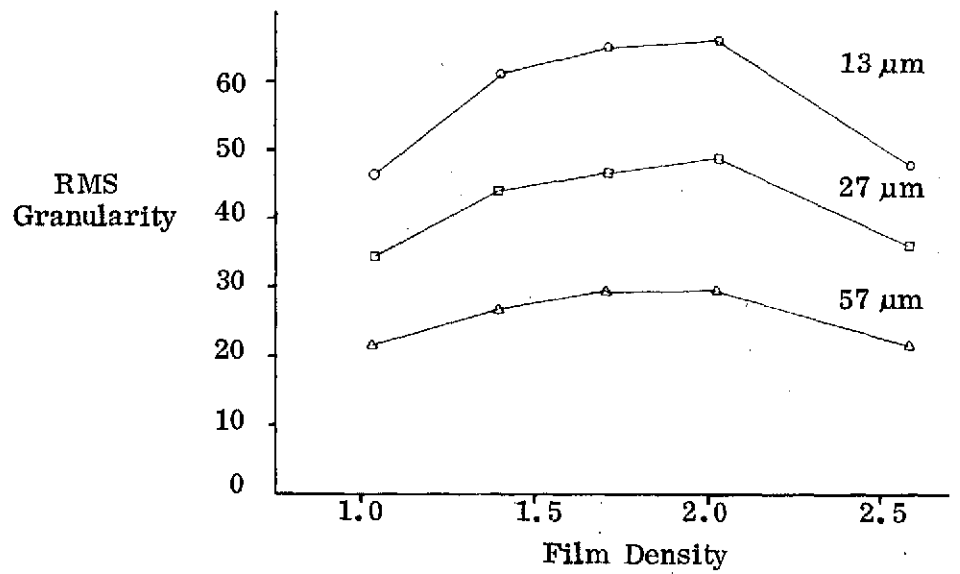

Figure 8. Comparison of RMS Granularity by Aperture for M, 200 keV, Fe (.25 inch)

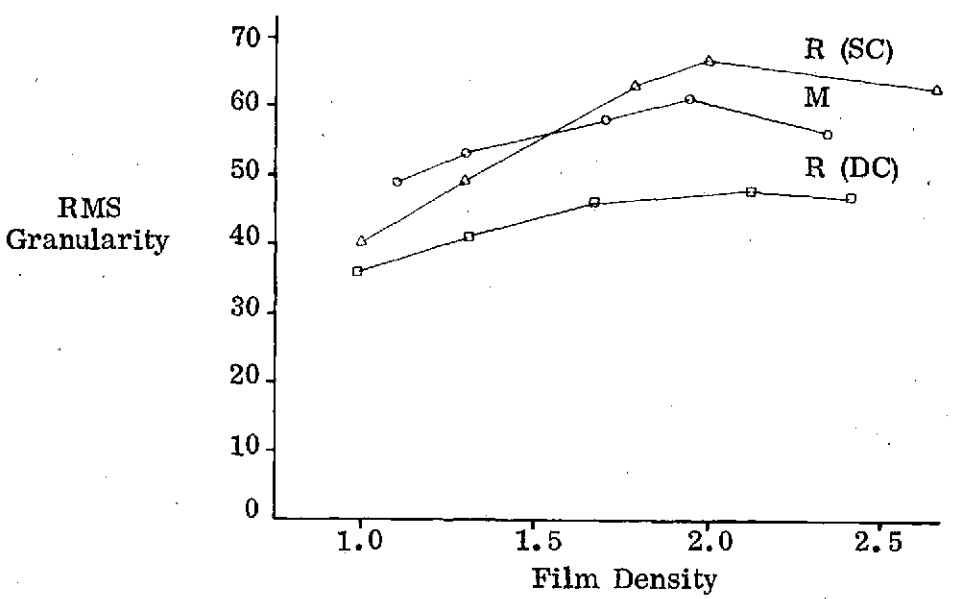

Figure 9. Comparison of Film Types at 100 keV, 13 μm Aperture

The type M film, which is also a double coat film, is shown to have a slightly higher granularity than the R (SC) film at the lower image densities. However, at the higher densities R (SC) has the higher granularity. Figures 10 and 11 show similar results for the three films when measured with the 27 and 57 micrometer apertures.

The data displayed in Figure 12 demonstrate that for radiographs produced with x-ray energies varying from 100 to 300 keV on the MG-150 device there was no appreciable change in the granularity. Although only data for R (DC) film is displayed, similar results were found for other two films as can be seen from the tables. Figure 13 illustrates that there is also no appreciable effect upon the film granularity due to the specimen type or thicknesses under consideration. Finally, the effect of lead intensifying screens is demonstrated in Figure 14. Although there were only a limited number of samples employing screens (three samples below 2.5 density) there apparently is no significant change in the granularity due to the lead screens.

2. Power Spectral Density Computations: The noise properties of selective radiographs were investigated by means of the PSD. The PSD estimates depict the spatial frequency power density for the noise processes examined. An in-depth examination of PSD can be found in Appendix III. The radiographs chosen for PSD analysis include all three film types, type M, R (SC), and R (DC). For each film type radiographs taken at 100 keV, 200 keV, and 300 keV were examined. For film types R (SC) and R (DC) radiographs at two low density levels were selected for analysis, and for film type M a range of density levels was chosen for each of the three energy levels. Those radiographs under consideration are listed in Table 21.

In presenting the results of the computations, the logarithms to the base 10 of the PSD's were computed and graphed as a function of spatial frequency. This was done so that the confidence intervals for the results could be given as straight lines on the graph. The upper and lower confidence interval curves are obtained by sliding the confidence interval lines over the computed results with the zero positioned on the curve and registering the values indicated at the endpoints of the arrows. For all PSD's presented, the resolution interval or bandwidth was approximately 5 cycles/mm. The results are presented in Figures 15-22. It should be noted that the PSD's are by definition normalized by the variance of the process so that the area under the curve is one. (In practice the value will be close to one.)

The shapes of the curves in Figures 15-22 are similar regardless of film type, energy level, or density level. However, the absolute magnitude of the power does change with the variance of the process. There is an apparent trend showing up as a decrease in the PSD values with increasing spatial frequency. This can be explained by the data collection scheme. The radiographs were scanned on the Mead Micro-Analyzer with a 12.5 micrometer aperture and 12 micrometer sampling interval.

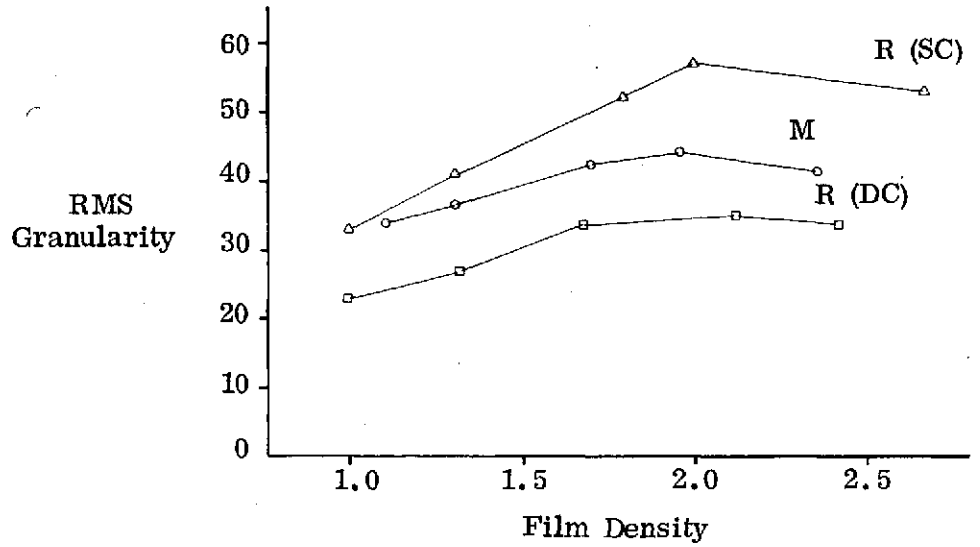

Figure 10. Comparison of Film Types at 100 keV, 27 μm Aperture

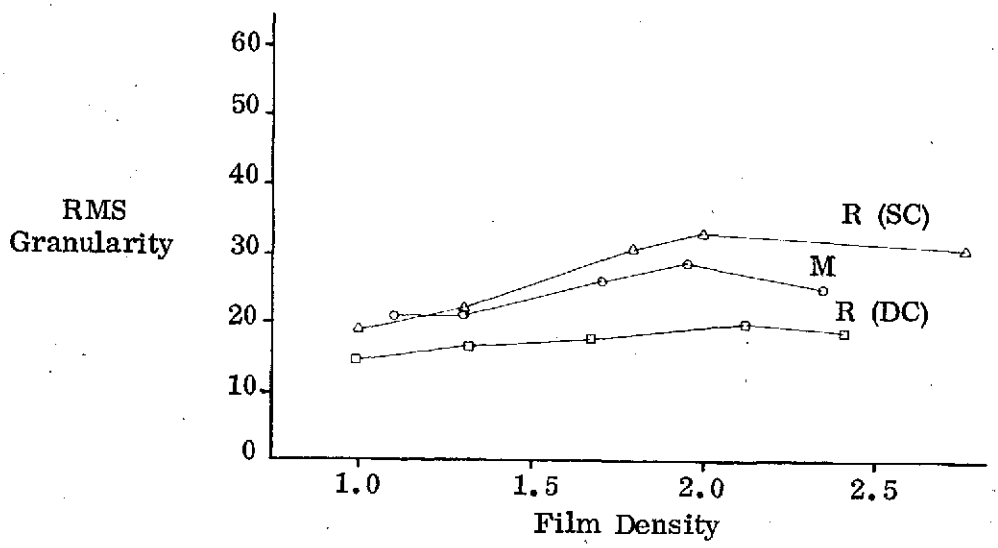

Figure 11. Comparison of Film Types at 100 keV, 57 μm Aperture

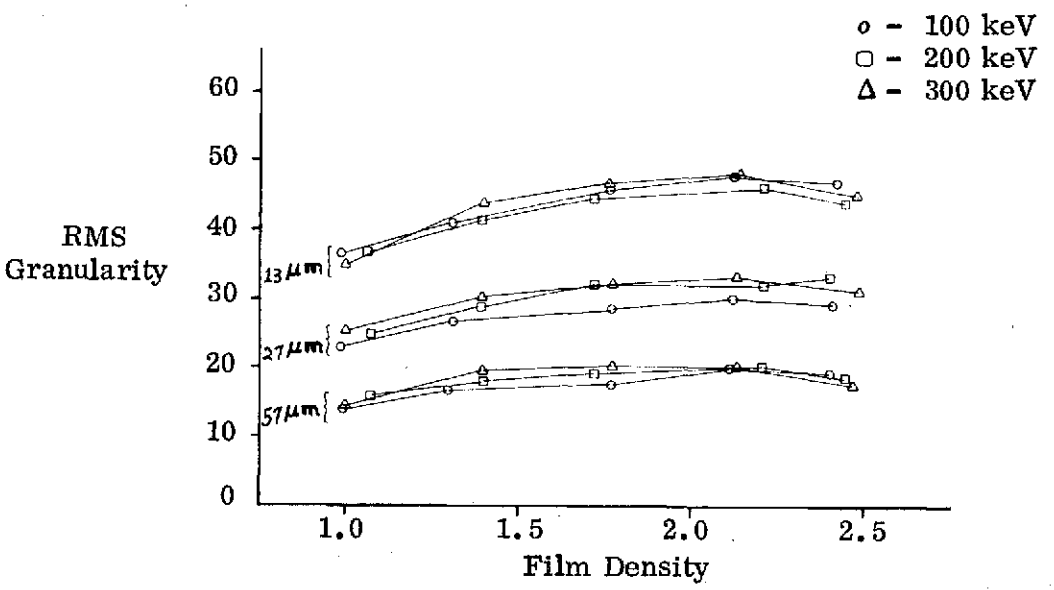

Figure 12. Comparison of RMS Granularity as a Function of keV for Film Type R (DC), for Aperture 13 μm, 27 μm, 57 μm

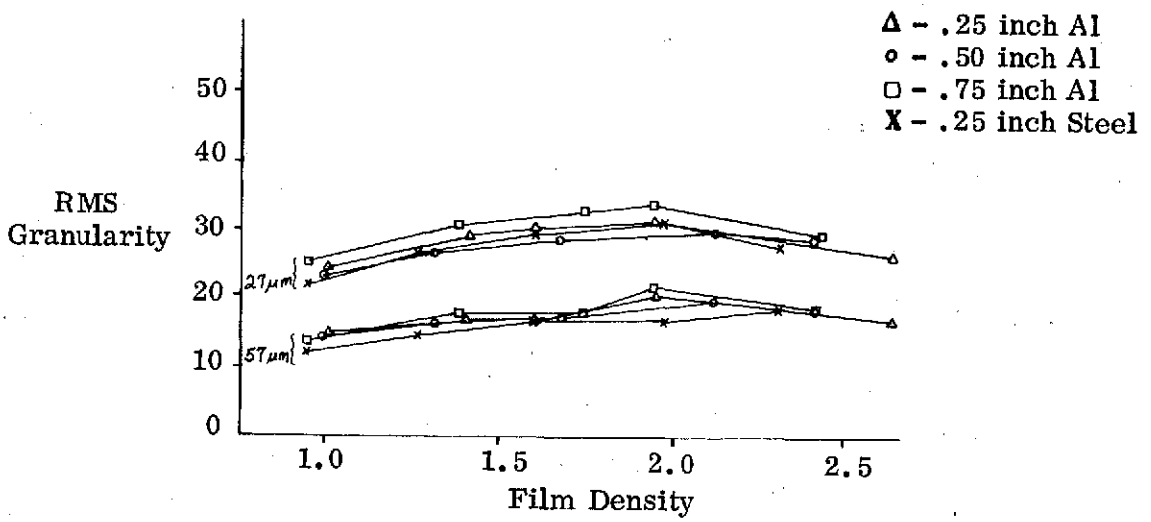

Figure 13. Comparison of RMS Granularity for Type R (DC) 100 keV as a Function of Specimen Material and Scanning Aperture

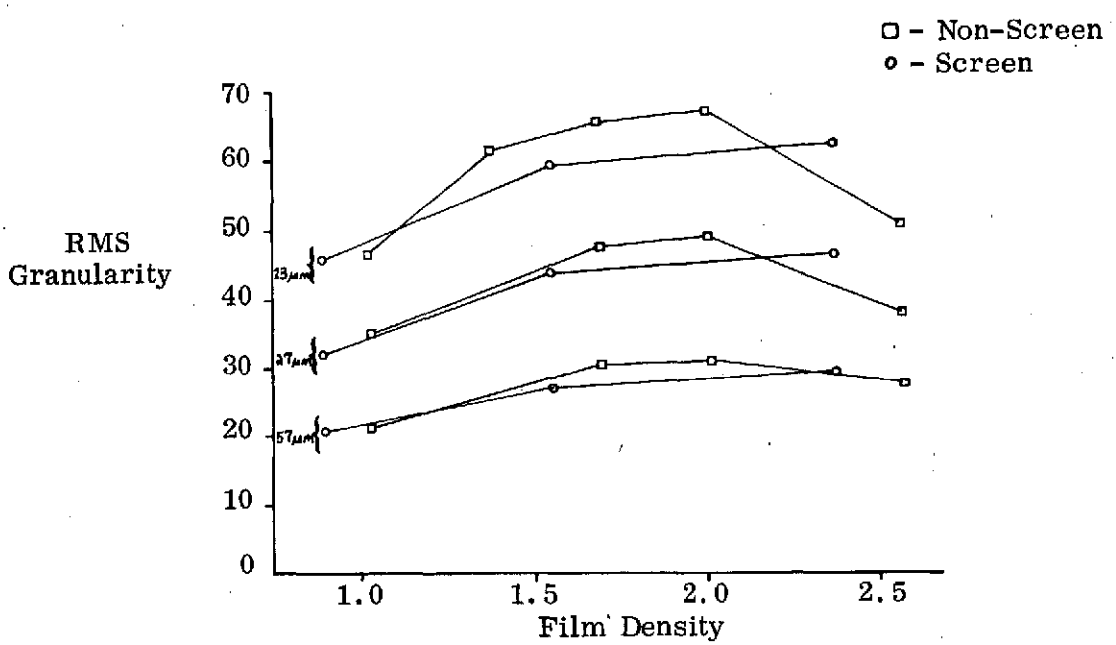

Figure 14. Effect of Intensifying Screens on RMS Granularity

Film Type	keV	Density Level
R (SC)	100	1.00
R (SC)	100	1.30
R (DC)	100	.99
R (DC)	100	1.31
M	100	1.10
M	100	1.30
M	100	1.69
M	100	1.95
R (SC)	200	.97
R (SC)	200	1.30
R (DC)	200	1.07
R (DC)	200	1.39
M	200	1.03
M	200	1.39
M	200	1.70
M	200	2.02
M	200	2.58
R (DC)	300	1.00
R (DC)	300	1.40
M	300	.98
M	300	1.35
M	300	1.81
M	300	2.18

Table 21. Radiographs Selected for PSD Analysis

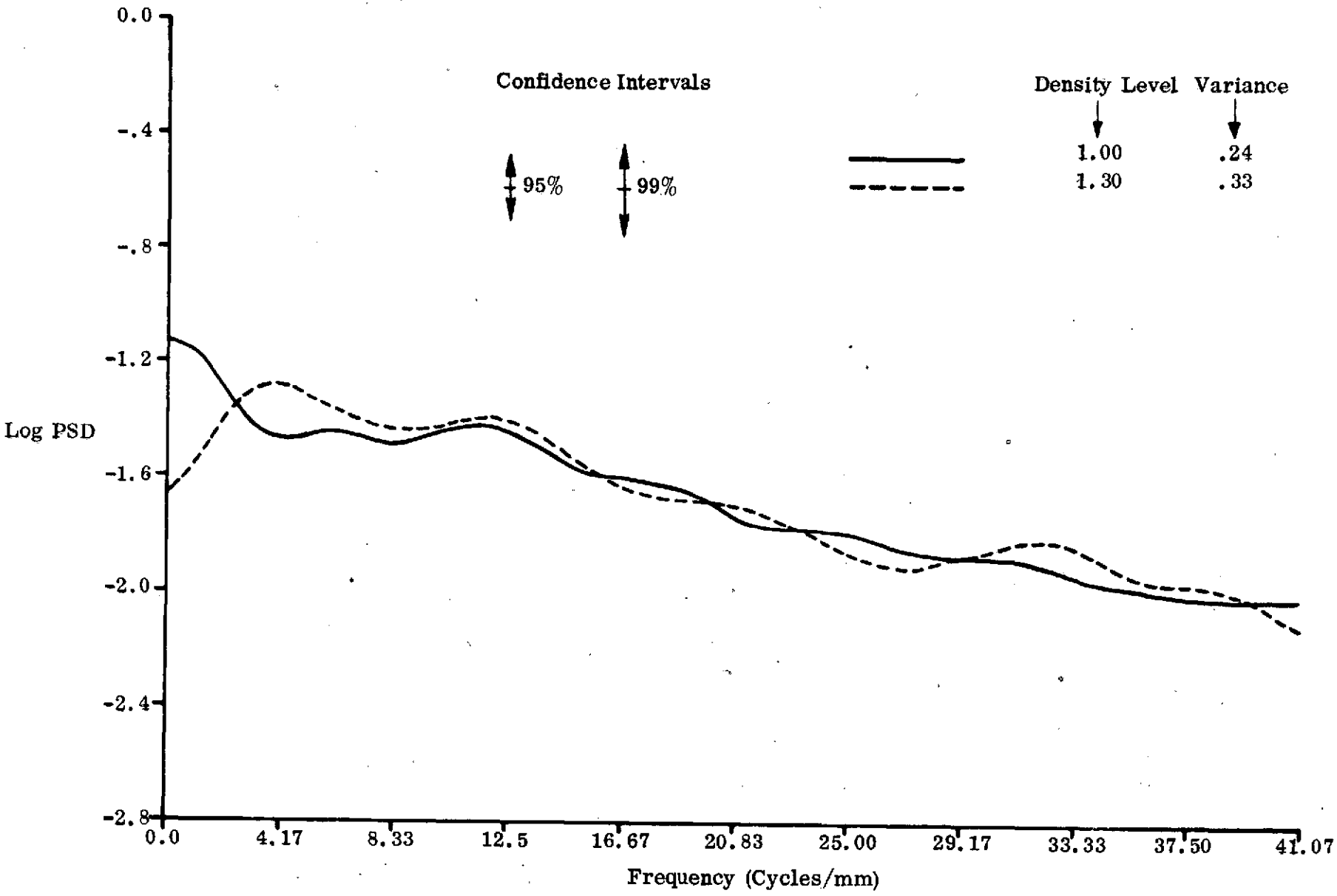

Figure 15. PSD R (SC), 100 keV

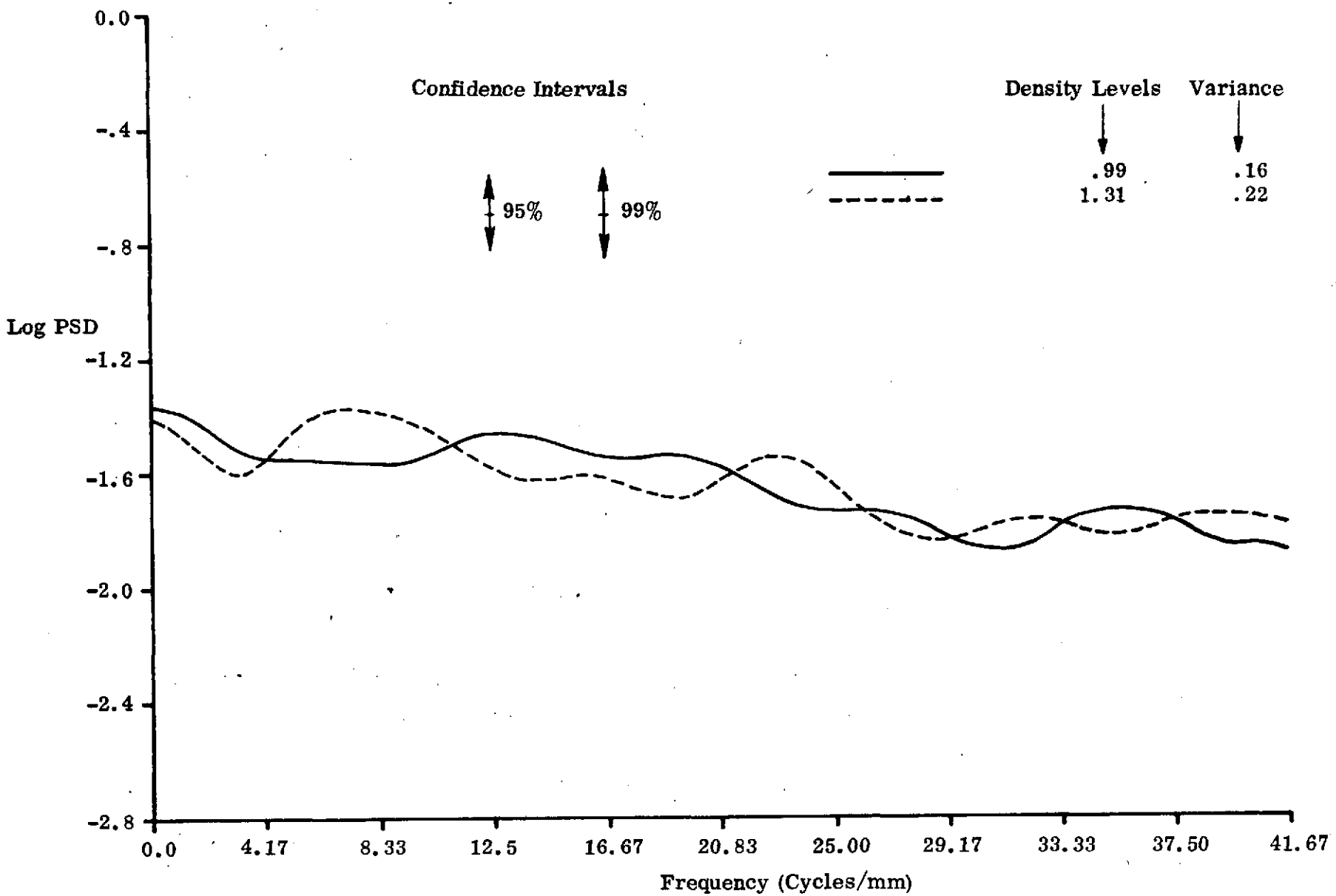

Figure 16. PSD R (DC), 100 keV

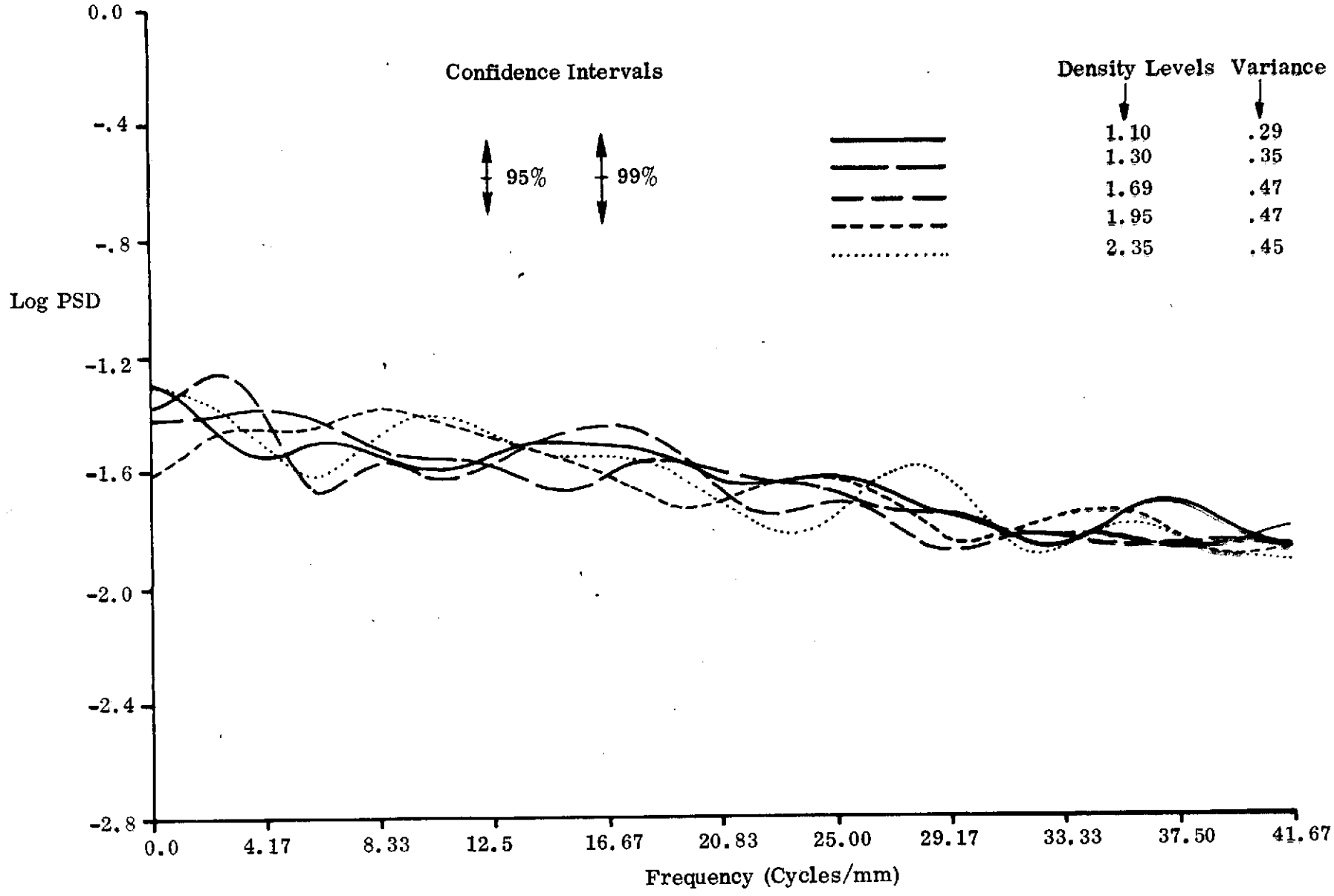

Figure 17. PSD M, 100 keV

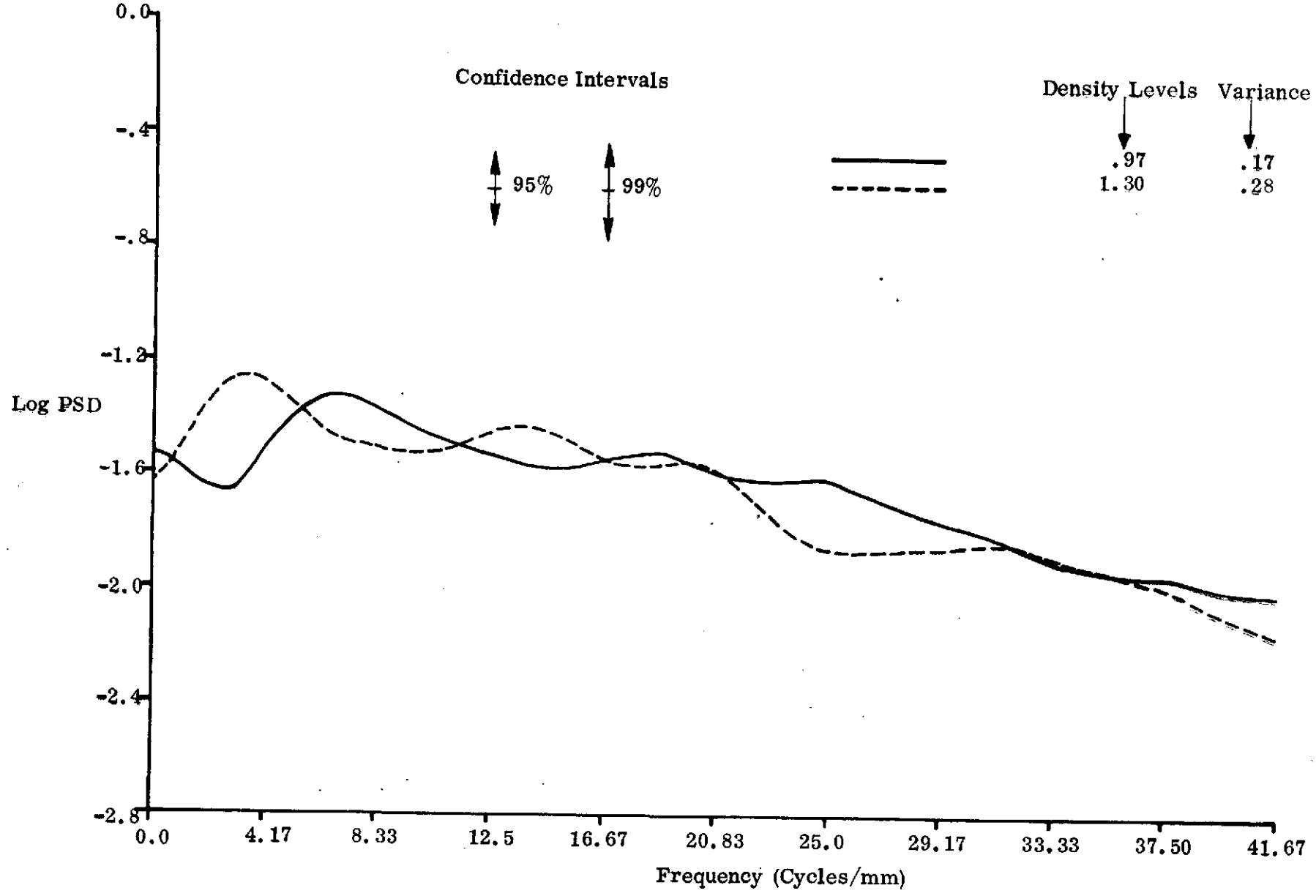

Figure 18. PSD R (SC), 200 keV

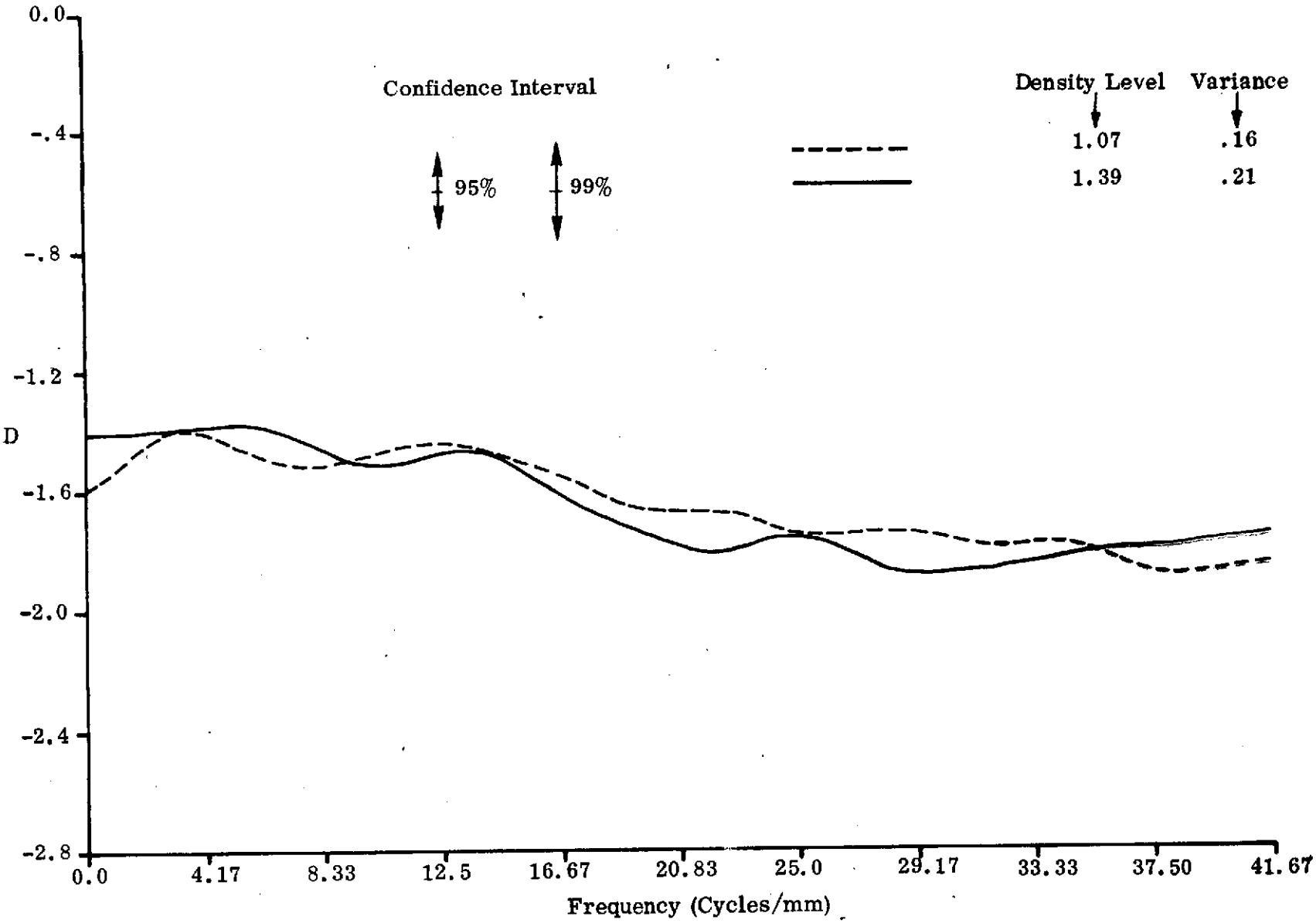

Figure 19. PSD R (DC), 200 keV

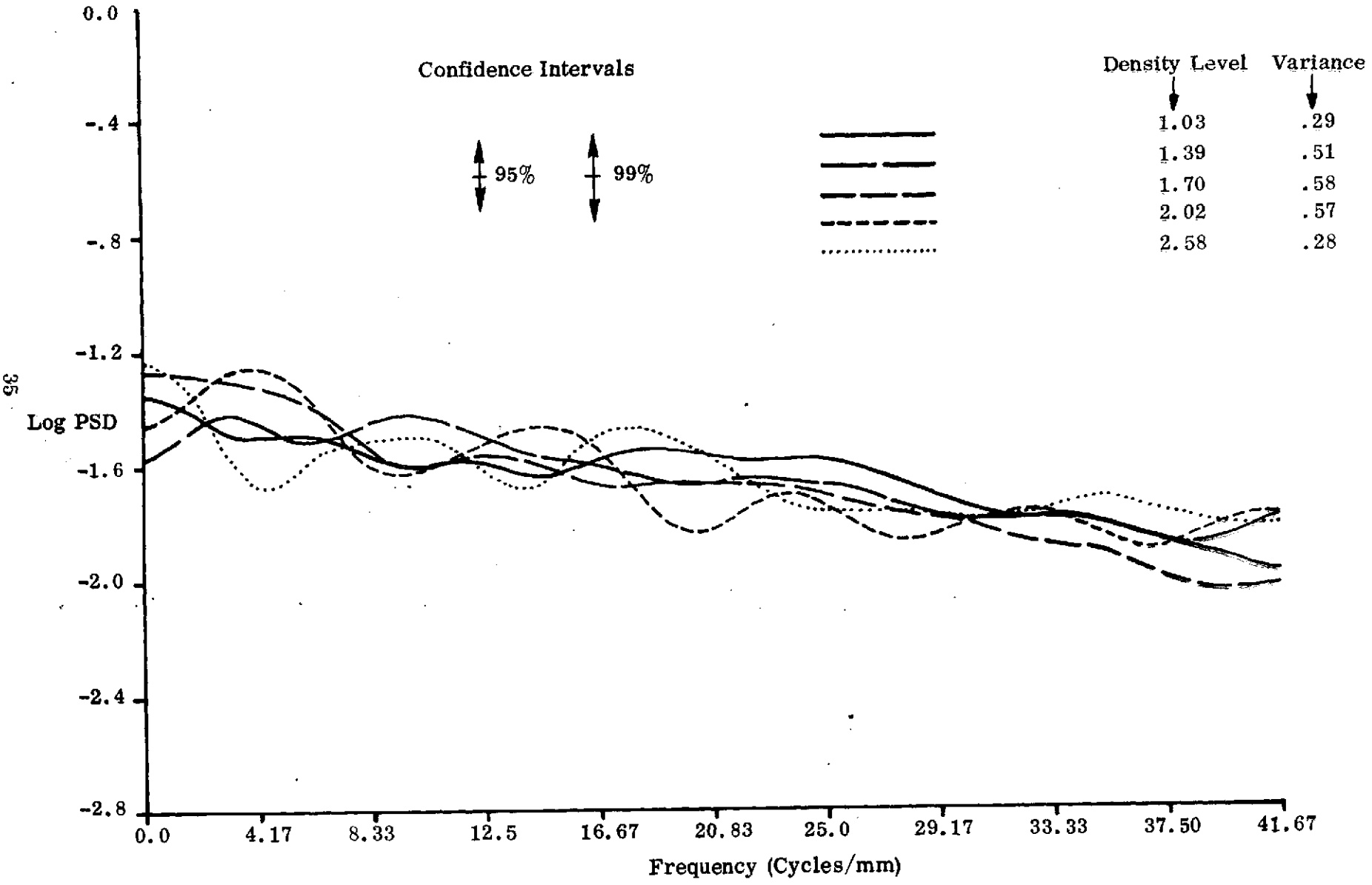

Figure 20. PSD M, 200 keV

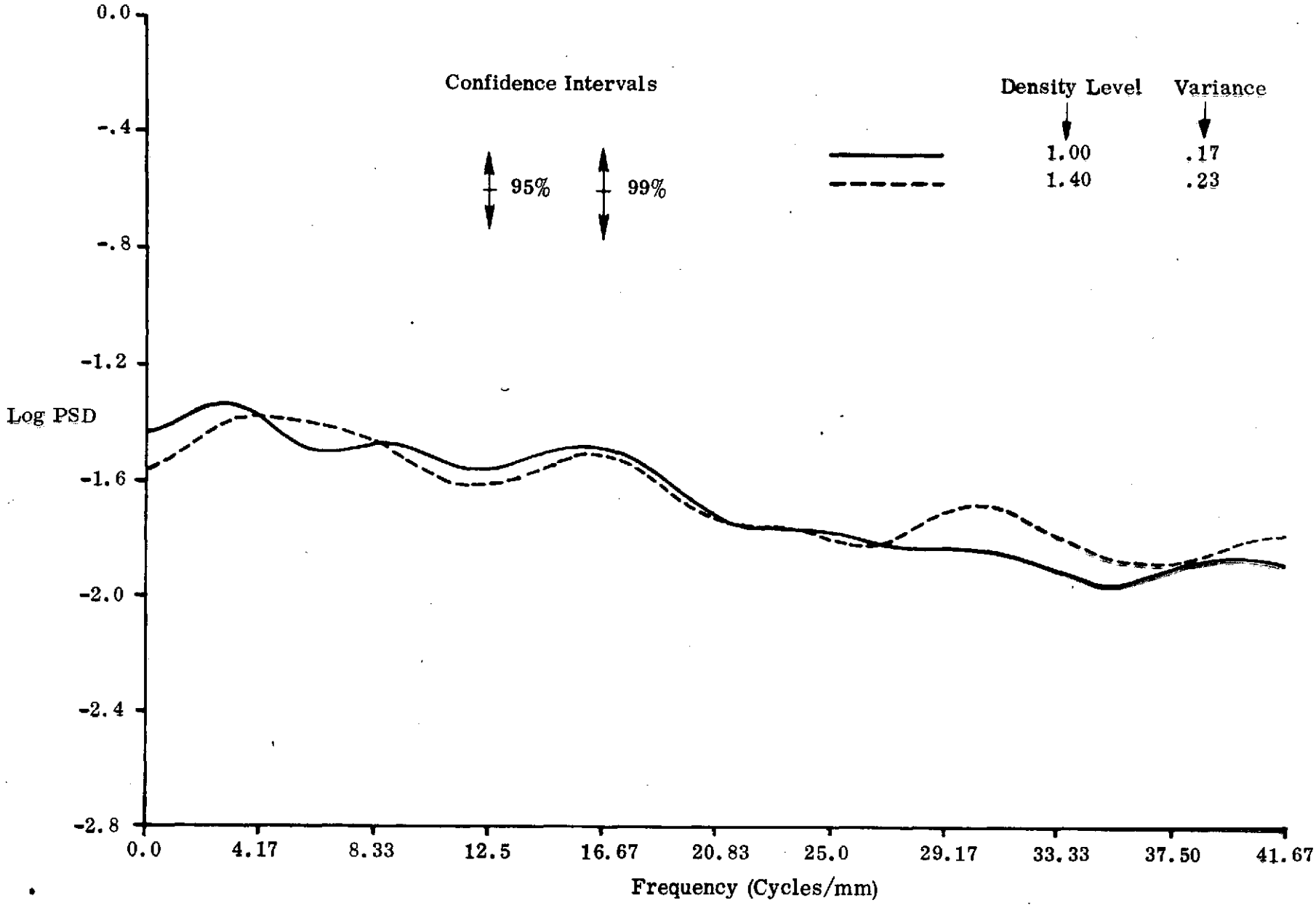

Figure 21. PSD R (DC), 300 keV

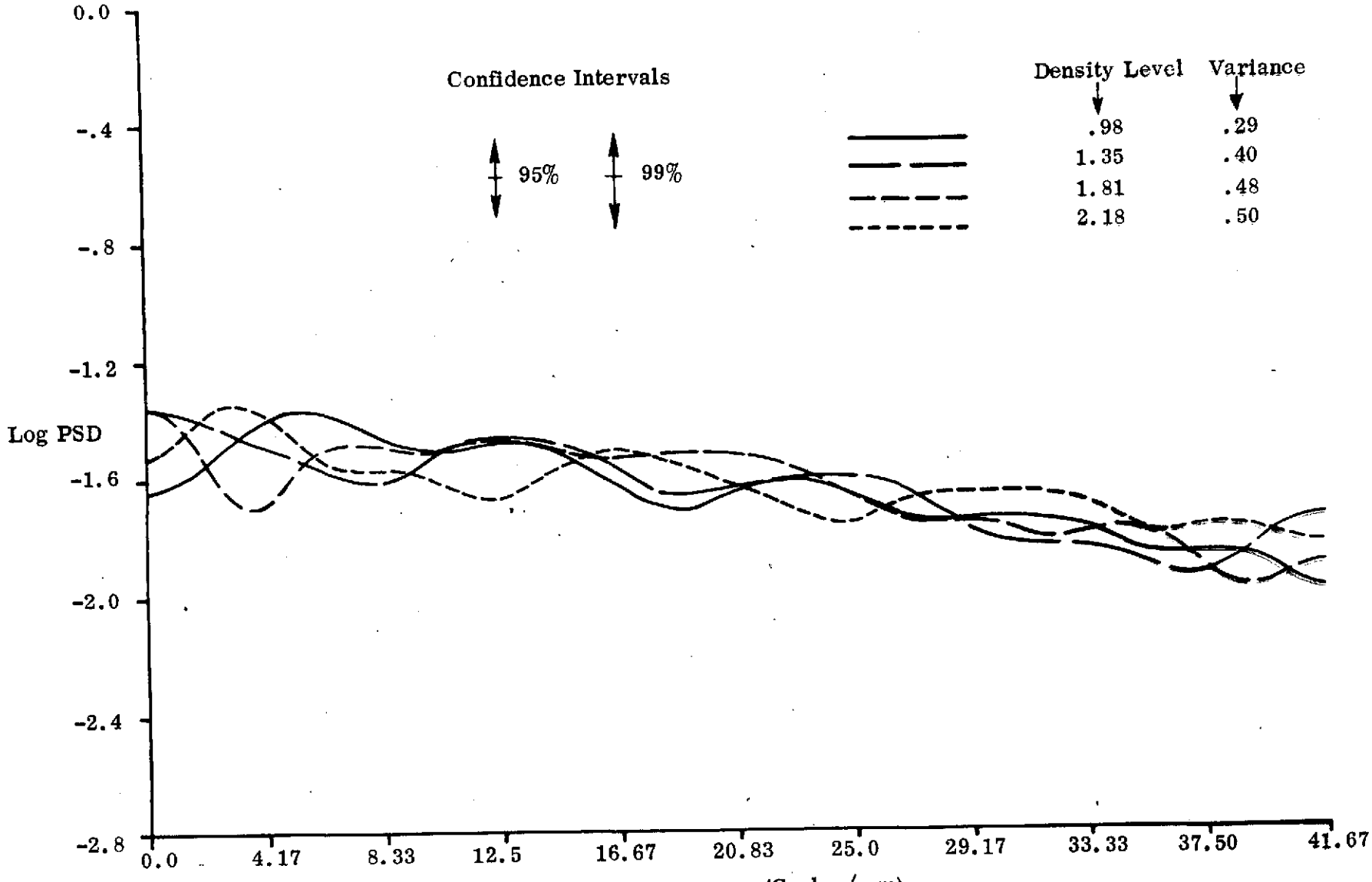

Figure 22. PSD M, 300 keV

The 12.5 micrometer aperture has a transfer function associated with it of the form

$$\frac{a^2 J_1 \ (2\pi\varrho a)}{\varrho}$$

where ϱ is the spatial frequency,
a is the radius of the aperture, and
J_1 is a Bessel function of order 1.

The cutoff frequency (zero of the Bessel function) occurs at approximately $1.2/2a \times 1000$ mm or $\frac{1200.0}{12.5} = 96.0$ cycles/mm. At 40.0 cycles/mm, the transfer function will decrease to approximately 0.7 the value at 0 cycles/mm. The PSD of the radiograph noise process, after smoothing by the aperture, is the product of the PSD of the radiograph process before smoothing and the square of the magnitude of the transfer function of the spot:

$$G_s(f) = G(F) \left| T(f) \right|^2$$

where $G_s(f)$ is the PSD of the process after smoothing,
$G^s(f)$ is the PSD of the process before smoothing, and
$T(f)$ is the transfer function of the spot.

The square of .7 is approximately .5. An examination of the smoothed PSD estimates shows that the values at 40 cycles/mm vary from approximately .2 to .7 times the values of the PSD's at very low frequencies. Taking the individual sample records as a group, the value of .5 probably represents a good approximation. In fact, using the log PSD values of -1.5 and -1.8, the ratio of the high to the low frequency PSD values is .5. Based on these results, it can reasonably be determined that before smoothing by the aperture the radiographic noise structure is indicative of white noise which is represented by a flat spectrum.

C. SCANNER NOISE

The noise properties of MSFC's Optronics scanner were investigated by operating the scanner with neutral-density (ND) filters as image specimens and recording the resulting digital information on magnetic tape. Both the magnitude and the power spectrum of the noise process present in the digital data were computed.

1. RMS Granularity Computation: The digital data collected from the scanner by digitizing the ten ND filters with apertures of 12.5 μm, 25 μm, and 50 μm were statistically analyzed to compute the mean digital step level and the standard deviation of the digital readouts per filter. The standard deviation was multiplied by one thousand in order to give a measure comparable to RMS granularity. Also, since this scanner records only sixty-four distinct density levels, whereas the Micro-Analyzer records two hundred-fifty-six levels, the standard deviation of the scanner noise process was converted to an effective RMS granularity number by multiplication by 4.25. This constant represents the slope of the scanner response curve, as the scanner response is compared against the ND filters.

The results of the statistical analysis of the scanner noise process for each aperture setting for each ND filter are shown in Table 22. The RMS granularity numbers generally follow the trend of decreasing with increased aperture given density level and increasing with increasing density for a given aperture. The exceptions of these trends can generally be regarded as points of indecision for the scanning device. That is, points where the ND filter level coincides with the boundary of one of the sixty-four selectable densities and where the device must make a continuing choice between two equally likely levels. The trends possessed by the scanner noise process can more readily be seen in the graphical representation of Figure 23.

2. PSD Computation: The noise properties of the scanner were additionally investigated through the computation of the power spectral density at each ND level. The results obtained by these computations are shown in Figures 24 and 25. It is obvious that there are large fluctuations present in the curves; and that some points of the graphs are off the scale. An examination of the PSD's also indicates large power at low frequencies, 0-5 cycles/mm. An examination of the results clearly shows that frequency periodicities were present in the data. These periodicities were not only showing up as large PSD values in the low frequency range but were also probably responsible for some of the extreme fluctuations in the PSD's. The density values of one of the records analyzed were examined and a dominant low frequency component was found. With this information Optronics scans of one of the granularity patches that was made at MSFC were analyzed for PSD. The parameters selected were film type M, energy level 100 keV, and density level 1.69D. The resulting PSD curves for three records of data can be found in Figure 26.

The same area on the granularity patch had previously been scanned by the Mead Micro-Analyzer and analyzed for PSD. The results of that analysis are shown in Figure 17. Comparison of these results with the ND filter analysis makes the following facts apparent: there is a similar large power at low frequencies in the PSD's obtained from an analysis of the Optronics noise characteristics and the PSD's obtained from the Optronics scan of the granularity patch but not in the PSD's obtained from the Mead Micro-Analyzer. This similarity in behavior rules out the possibility that the cause of the high power at low frequency is due to the ND filters. The only remaining feasible alternative is that the Optronics scanner was not operating correctly and was contaminating the data by generating low frequency periodicities.

D. IMAGE DEGRADATION

The image degradation of the entire x-ray/scanner system was computed by examining the system's MTF as measured by edge gradient analysis. A complete description of the techniques employed in this type analysis can be found in Appendix IV.

1. Edge Selection: The edge target provided for seven edges as candidates for analysis. These edges can be identified by a lower density step level and an upper density step level. The identification chosen for these edges is presented in Table 23.

Filter Density	Optronics Digital Mean Value			1000 x Standard Deviation			RMS Granularity		
	12.5 μm	25 μm	50 μm	12.5 μm	25 μm	50 μm	12.5 μm	25 μm	50 μm
0.18	0.8	2.0	3.0	2	0	0	9.5	0	0
0.48	6.8	8.4	9.0	3	1.75	0	12.75	7.44	0
0.82	14.6	16.7	17.0	2	1.5	1	9.5	6.38	4.25
0.98	17.9	19.8	20.3	3	2.25	3.25	12.75	5.06	13.8
1.16	20.4	22.9	24.0	3-3/4	3	1	15.94	12.75	4.25
1.50	28.2	30.5		2.5	4.25		14.9	19.13	
1.76	35.5	37.0	38.0	4.5	3.3	3.0	19.13	14.03	12.75
1.94	41.1	42.5	43.0	4.0	3.0	2.0	17	12.75	8.5
2.19	44.7	47.4	48.1	3.3	3.7	3.9	14.03	15.73	16.58
2.39	51.1	53.1	53.0	3.0	3.7	4.0	12.75	15.73	17

Table 22. MSFC Optronics Noise Process RMS Granularity

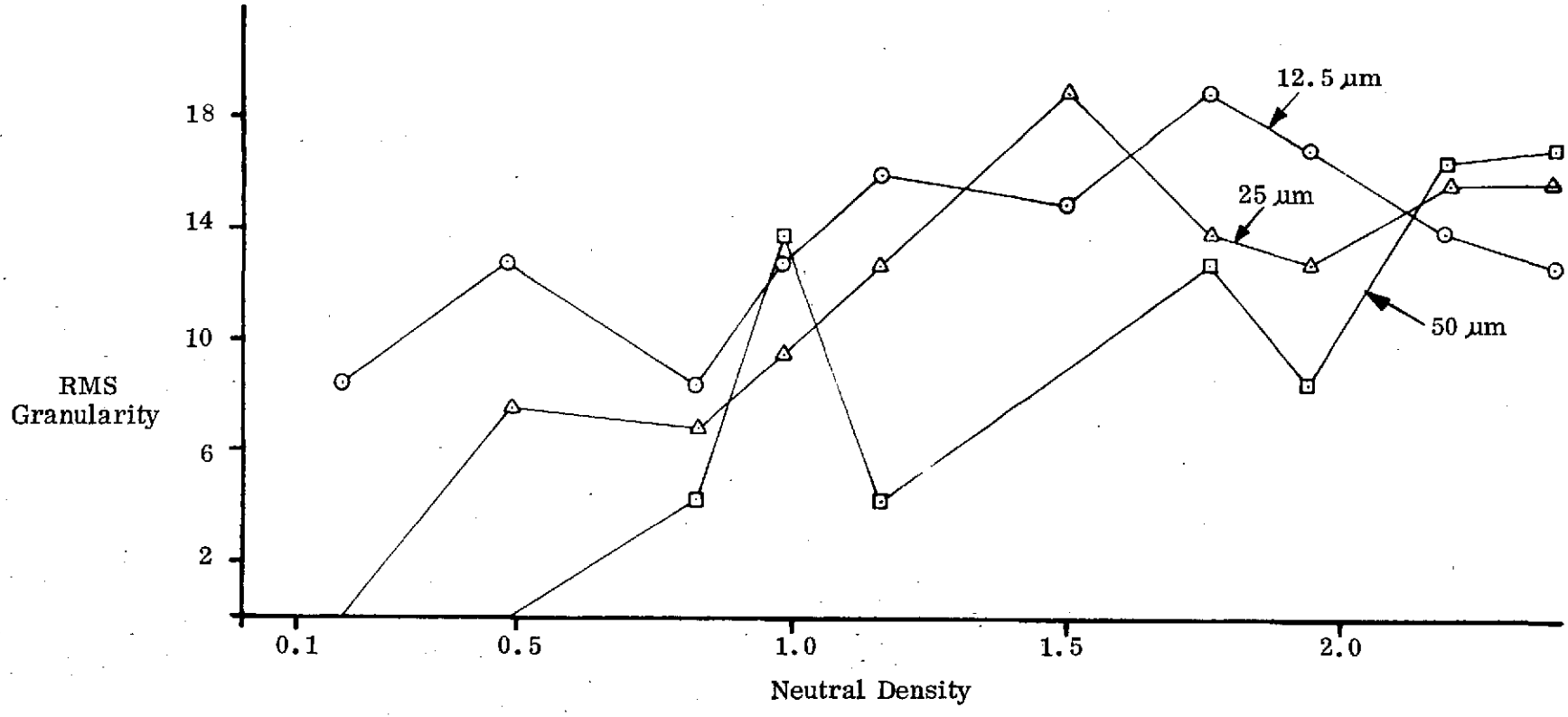

Figure 23. Graphical Display of MSFC Scanner Noise Magnitude

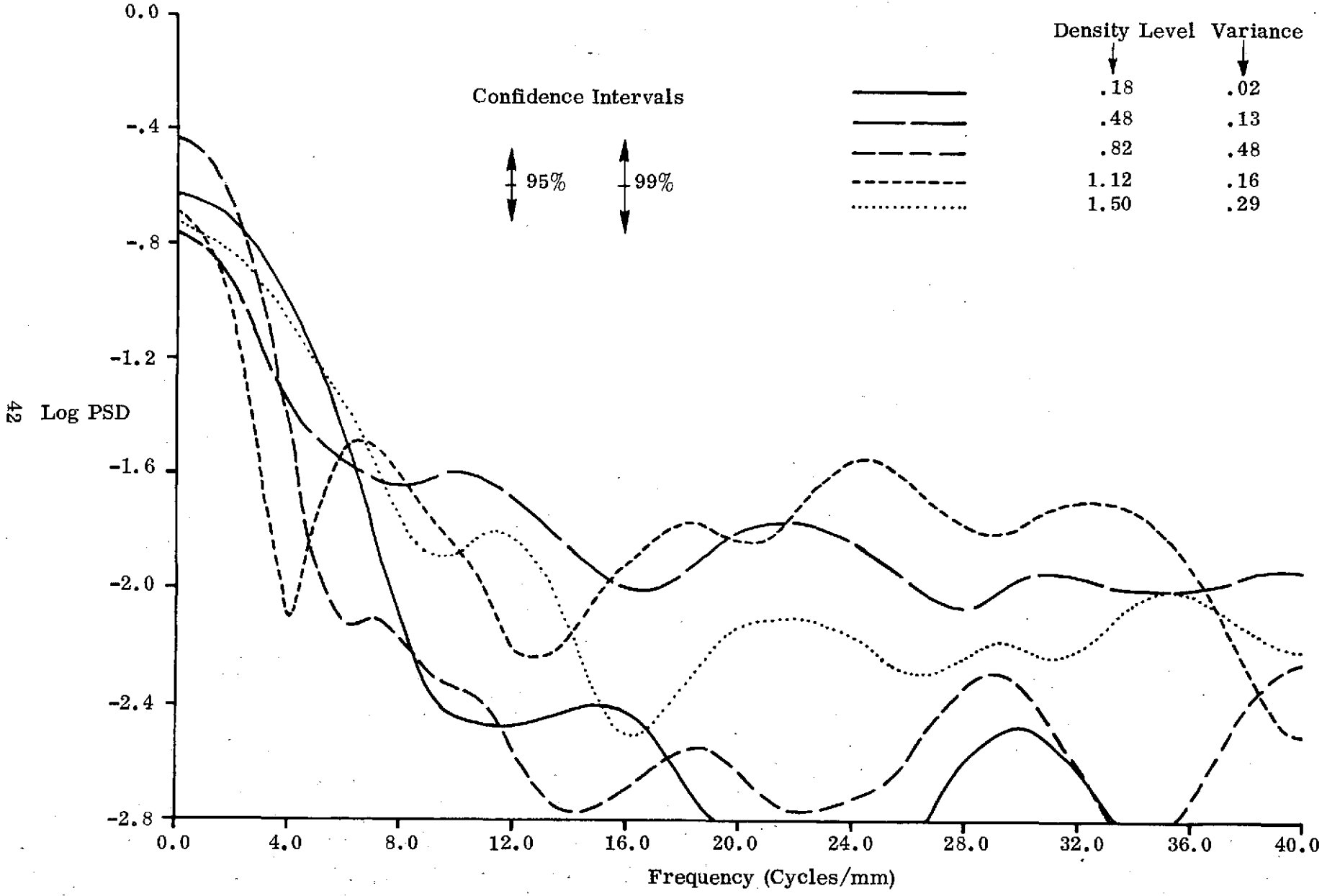

Figure 24. PSD MSFC's Scanner Density Levels, .18, .45, .82, 1.12, 1.50 (12.5 μm Aperture)

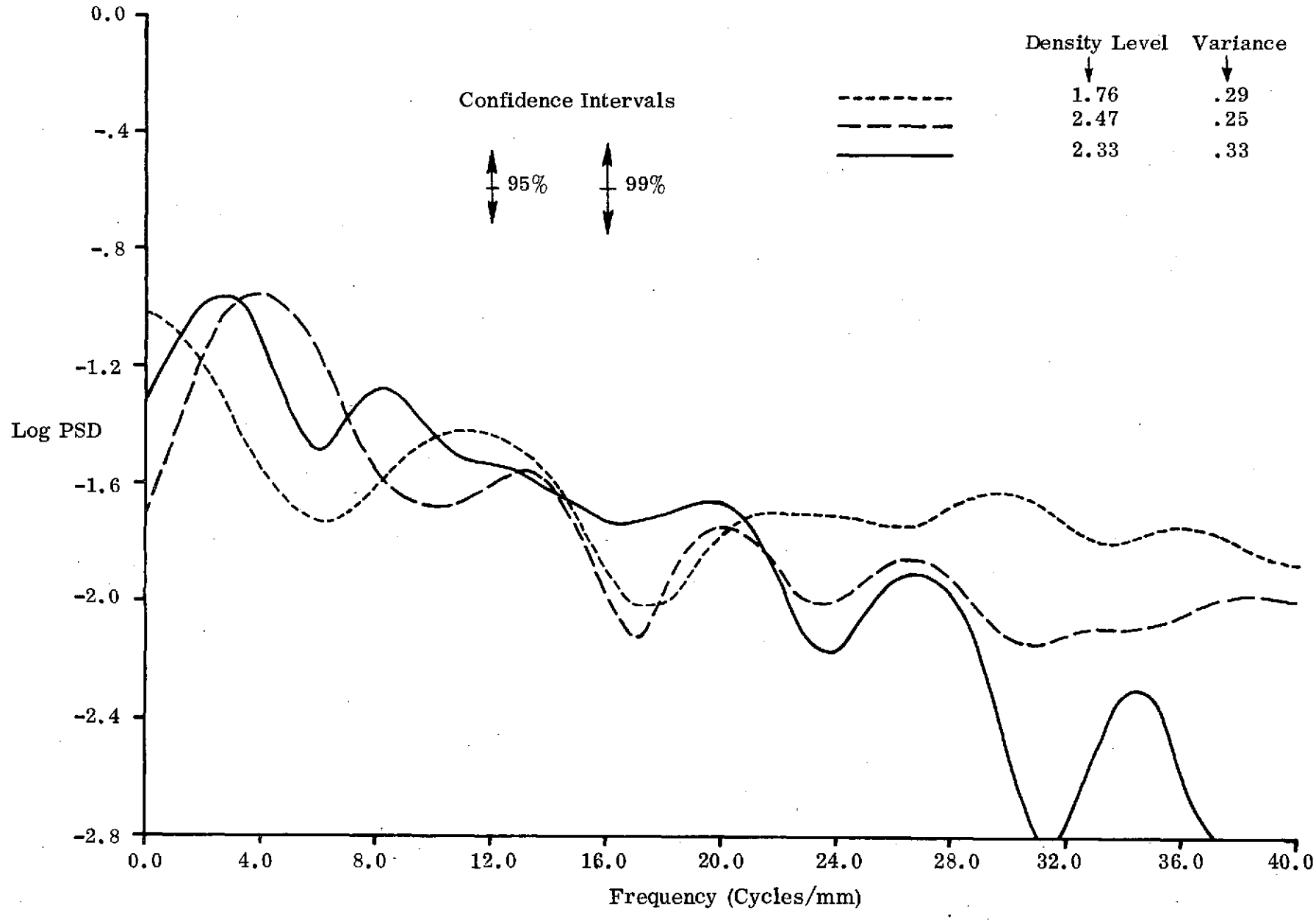

Figure 25. PSD MSFC's Scanner Density Levels 1.76, 2.47, 2.33 (12.5 μm Aperture)

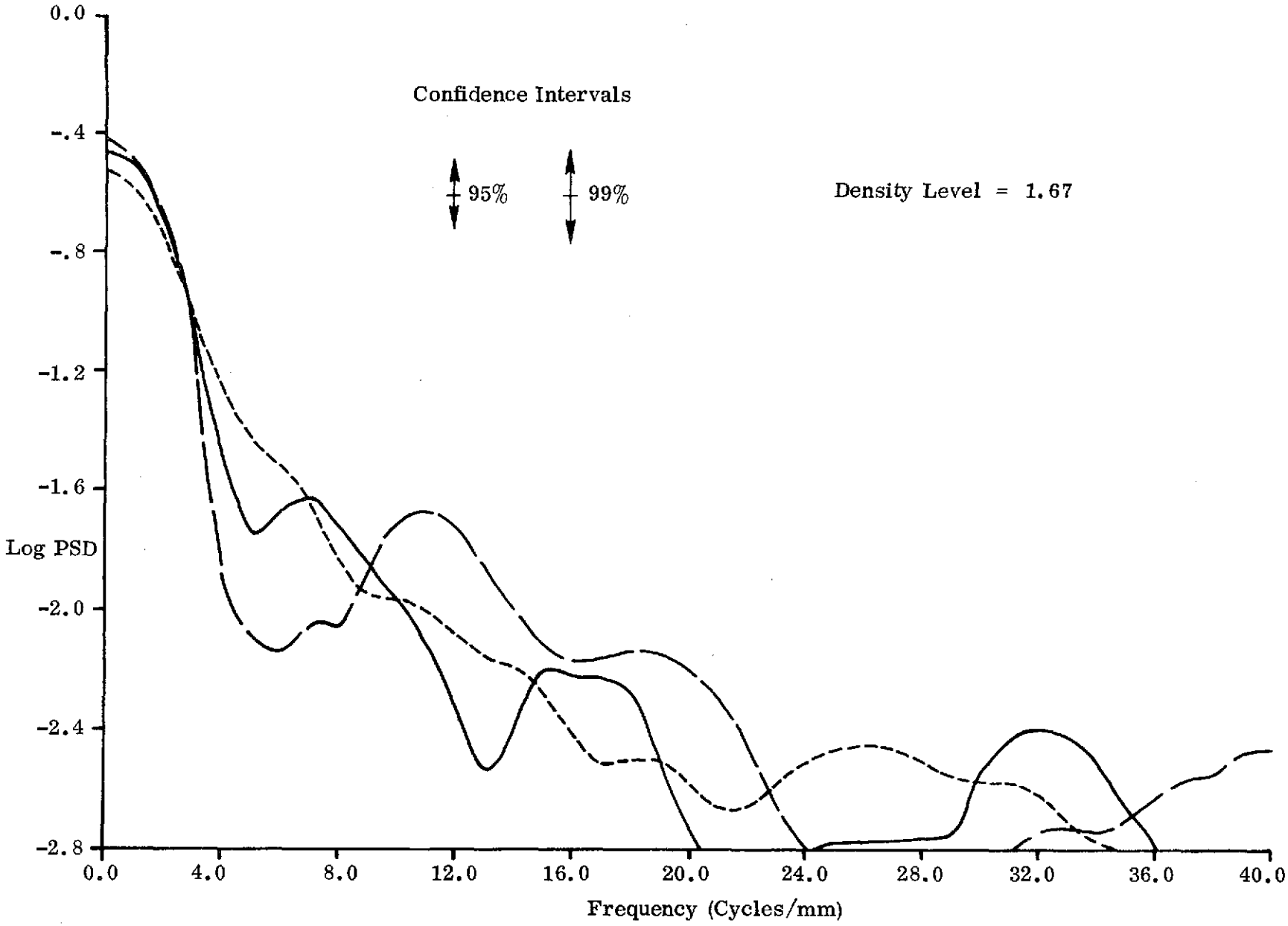

Figure 26. PSD of Type M Film, 100 keV Scanned at MSFC (12.5 μm Aperture)

Edge No.	Lower Step	Upper Step
1	1	2
2	2	3
3	3	4
4	4	5
5	5	6
6	6	7
7	7	8

Table 23. Edge Identification

The nine exposures generated for MTF analysis presented a total of sixty-three edges for analysis. However, many of the edges had density differences so low that the Optronics scanner was unable to detect the edge response. The result was twenty-six analyzable edges. The particular edges which were detected by the scanner are found in Table 24.

Exposure Identification	Edge No. 1	2	3	4	5	6	7
100-2-2.5			X		X		X
70-3-2			X		X		X
200-1-1			X		X		X
100-1-4.2			X		X		X
100-3-1			X		X		X
200-1-1.5			X		X		X
80-3-2			X		X		X
100-1-4					X		X
100-3-1.5			X		X		X

Table 24. Edge Responses Suitable for Analysis

2. MTF Computation: From each of the twenty-six edge responses a representative MTF was computed. Each representative MTF was the average of six MTF's computed from various locations on the edge. Approximately one hundred digital data records were collected from three positions on the edge. Each of the sets of one hundred were divided into two groups of fifty adjacent records. Each group of fifty records presented data for one MTF estimate. Hence, for each edge six MTF estimates were computed. The six MTF estimates per edge were then averaged yielding a representative MTF for the edge. The twenty-six representative MTF's can be found in Table 25.

All of the computed MTF's fell into the narrow envelope shown in Figure 27. Thus, regardless of the film type, energy level, exposure time or format position under consideration, the MTF for the system can be found to lie in the envelope. The narrowness of the envelope indicates that the MTF of the x-ray/scanner system is relatively independent of the variables considered in the experiment.

Frequency	Modulation Transfer Edge No. 3	Modulation Transfer Edge No. 5	Modulation Transfer Edge No. 7
0	1.00	1.00	1.00
2	0.91	0.93	0.89
4	0.71	0.80	0.67
6	0.52	0.66	0.44
8	0.33	0.48	0.24
10	0.16	0.25	0.14
12	0.07	0.07	0.08
14	0.06	0.14	0.03
16	0.06	0.13	0.05

25a. Exposure 80-3-2

Frequency	Modulation Transfer Edge No. 3	Modulation Transfer Edge No. 5	Modulation Transfer Edge No. 7
0	1.00	1.00	1.00
2	0.91	0.95	0.91
4	0.73	0.82	0.91
6	0.54	0.67	0.40
8	0.34	0.49	0.19
10	0.16	0.29	0.09
12	0.06	0.14	0.11
14	0.03	0.12	0.10
16	0.04	0.12	0.07

25b. Exposure 100-2-2.5

Frequency	Modulation Transfer Edge No. 3	Modulation Transfer Edge No. 5	Modulation Transfer Edge No. 7
0	1.00	1.00	1.00
2	0.93	0.94	0.94
4	0.77	0.78	0.81
6	0.58	0.58	0.65
8	0.36	0.37	0.47
10	0.15	0.19	0.26
12	0.07	0.09	0.09
14	0.08	0.10	0.12
16	0.08	0.10	0.12

25c. Exposure 70-3-2

Table 25. MTF's for Twenty-Six Edges
(1 of 3)

Frequency	Modulation Transfer Edge No. 3	Modulation Transfer Edge No. 5	Modulation Transfer Edge No. 7
0	1.00	1.00	1.00
2	0.88	0.87	0.88
4	0.71	0.59	0.61
6	0.53	0.35	0.40
8	0.32	0.25	0.30
10	0.16	0.19	0.18
12	0.13	0.20	0.08
14	0.08	0.19	0.09
16	0.08	0.15	0.13

25d. Exposure 200-1-1

Frequency	Modulation Transfer Edge No. 3	Modulation Transfer Edge No. 5	Modulation Transfer Edge No. 7
0	1.00	1.00	1.00
2	0.91	0.90	0.92
4	0.70	0.70	0.72
6	0.46	0.56	0.46
8	0.27	0.45	0.24
10	0.14	0.26	0.10
12	0.06	0.08	0.07
14	0.06	0.11	0.07
16	0.06	0.08	0.06

25e. Exposure 100-1-4.2

Frequency	Modulation Transfer Edge No. 3	Modulation Transfer Edge No. 5	Modulation Transfer Edge No. 7
0	1.00	1.00	1.00
2	0.94	0.91	0.93
4	0.78	0.68	0.73
6	0.55	0.40	0.48
8	0.31	0.19	0.25
10	0.11	0.11	0.11
12	0.06	0.10	0.09
14	0.08	0.08	0.10
16	0.06	0.08	0.08

25f. Exposure 100-1-4

Table 25. MTF's for Twenty-Six Edges
(2 of 3)

Frequency	Modulation Transfer Edge No. 3	Modulation Transfer Edge No. 5	Modulation Transfer Edge No. 7
0	1.00	1.00	1.00
2	0.92	0.90	0.90
4	0.71	0.70	0.66
6	0.50	0.56	0.45
8	0.31	0.44	0.32
10	0.16	0.26	0.18
12	0.07	0.18	0.12
14	0.06	0.21	0.08
16	0.09	0.16	0.07

25g. Exposure 100-3-1

Frequency	Modulation Transfer Edge No. 3	Modulation Transfer Edge No. 5	Modulation Transfer Edge No. 7
0	1.00	1.00	1.00
2	0.90	0.90	0.90
4	0.68	0.68	0.69
6	0.46	0.46	0.38
8	0.29	0.29	0.29
10	0.16	0.16	0.13
12	0.08	0.08	0.09
14	0.05	0.05	0.10
16	0.04	0.04	0.09

25h. Exposure 200-1-1.5

Frequency	Modulation Transfer Edge No. 3	Modulation Transfer Edge No. 5	Modulation Transfer Edge No. 7
0	1.00	1.00	1.00
2	0.92	0.93	0.88
4	0.73	0.77	0.63
6	0.50	0.61	0.41
8	0.29	0.44	0.25
10	0.15	0.24	0.12
12	0.05	0.10	0.08
14	0.07	0.12	0.07
16	0.06	0.11	0.05

25i. Exposure 100-3-1.5

Table 25. MTF's for Twenty-Six Edges
(3 of 3)

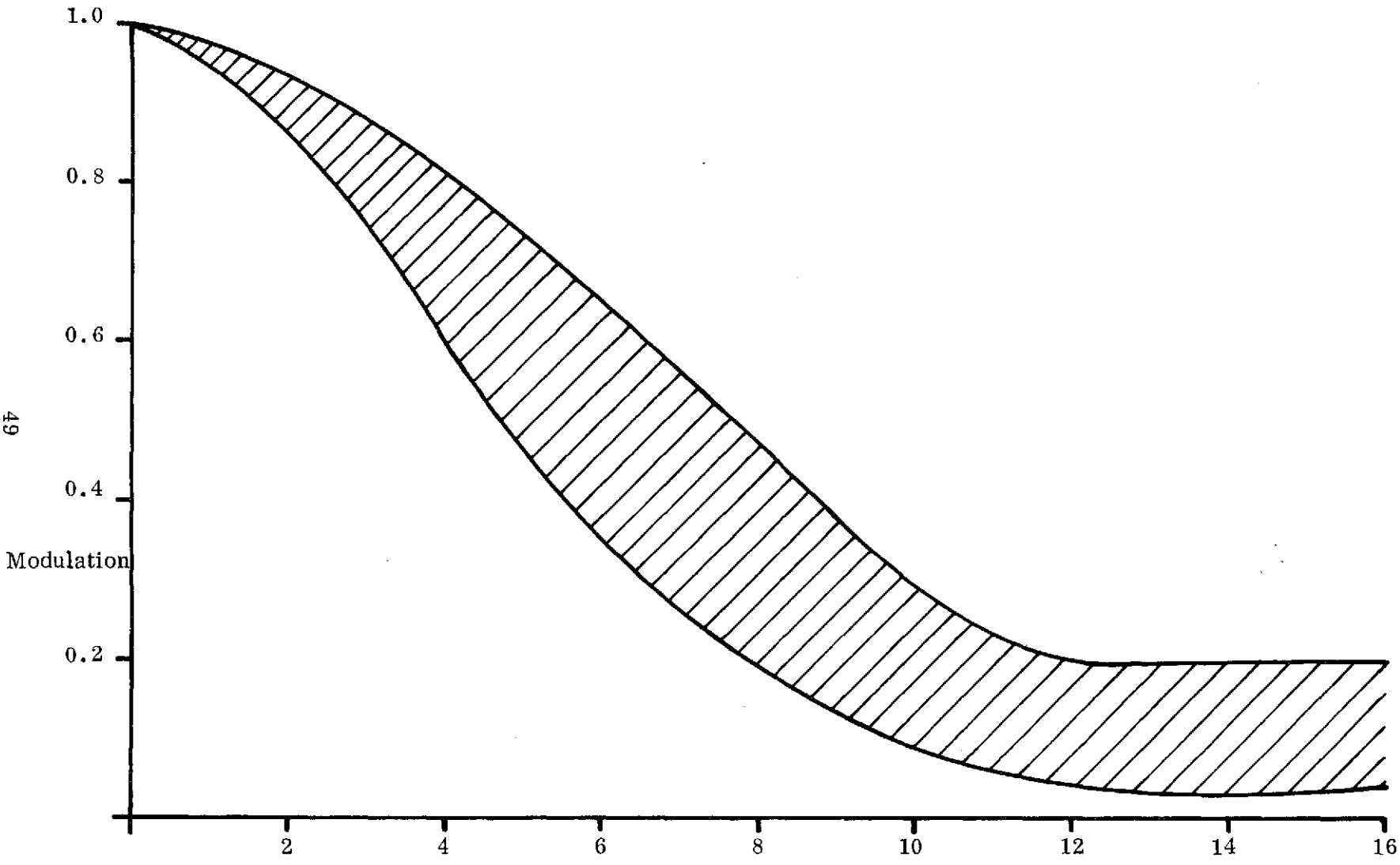

Figure 27. Envelope Curve of MTF's

SECTION IV

CONCLUSIONS & RECOMMENDATIONS

A. CONCLUSIONS

This program investigated four areas to be considered by MSFC when engaging in digital image enhancement of weld flaws through the application of digital filtering techniques to radiographic imagery scanned on the Optronics microdensitometer. Three of these areas film granularity, quantum mottle and the scanning process were considered as potential noise sources and quantified by RMS granularity numbers and/or the process' power spectrum (PSD). The fourth area of investigation was the image degradation introduced by the combination of x-ray source, film and scanning device. The performance of these combined elements was measured through computation of the system's MTF.

Quantitative analysis of these four areas has indicated the following:

1. For a fixed film type and density level, the film graininess decreased as the aperture size increased.

2. For a fixed film type and aperture size, the film graininess was seen to increase as density increased up to approximately 2.0D where graininess began to decrease.

3. Type R (DC) film demonstrated the lowest RMS granularity level over the specified density range.

4. No appreciable variation in RMS granularity of quantum mottle (including film grain) was detected for x-ray energies in the 100 to 300 keV range on the MG-150 device.

5. RMS granularity for quantum mottle (including film grain) at a specific density level did not change as a result of varying specimen thickness or material type.

6. The quantum mottle (including film grain) noise process for each film type was approximately "white".

7. Trends or low spatial frequencies were introduced into digital data by the Optronics scanner.

8. The sixty-four levels of digital output from the Optronics scanner were not sufficient to distinguish the low modulation edges or flaws.

9. The family of MTF's generated under varying conditions fell into a relatively narrow envelope indicating general independence of the system MTF on film type, energy level and format position.

B. RECOMMENDATIONS

For a particular application of filtering to radiograph enhancement,it may be possible to reduce the effect of the film grain noise by bandpass spatial filtering. This could be accomplished by suppressing high spatial frequencies in the data. Great care should be taken since such "low-pass" spatial filtering will also blur the image, which is usually undesirable. However, it is quite possible to suppress noise from a radiograph by deleting a selected band of spatial frequencies while leaving enough at high frequencies to maintain sharp edges. Since there is no dominant band of spatial frequencies in the film grain noise process investigated, the effect of this type of filtering would have to be related to the image of interest and type of information desired.

The trends or low frequencies introduced by the Optronics scanner present special problems. Any attempt to filter out these low frequency components would distort most images beyond recognition. Removal of such trends, if possible, would have to be done spatially on a point by point basis. This, in turn, requires exact knowledge of the trend introduced by the scanner.

The MTF curve envelope indicates that image enhancement through a restoration process could be accomplished through the application of a single filter independent of the film type, energy level or format position within the ranges considered in this study. A representative MTF belonging to the generated family could be employed for restoration.

SECTION V

BIBLIOGRAPHY

1. Blackman, R. B. and Tukey, J. W., The Measurement of Power Spectra, Dover Publishing Co., New York, 1958.

2. Clark, G. L., Applied X-Rays (Fourth Edition), McGraw-Hill Book Co., New York, 1955.

3. Radiography in Modern Industry (Third Edition), Eastman-Kodak Co., Rochester, 1969.

4. Herz, R. H., The Radiographic Action of Ionizing Radiations, Wiley-Interscience, New York, 1969.

5. Hinsley, J. F., Nondestructive Testing, Gordon and Breach Science Publishers Inc., New York, 1959.

6. Jenkins, G. M. and Wahs, D. G., Spectral Analysis and Its Applications, Holden-Day, San Francisco, 1968.

7. Morgan, R. H. and Corrigan, K. E., (editors), Handbook of Radiology, The Leer Book Publishers Inc., Chicago, 1955.

8. Rickmers, A. D. and Todd, H. N., Statistics: An Introduction, McGraw-Hill Book Co., New York, 1967.

9. Scott, W. G. (editor), Planning Guide for Radiologic Installations (Second Edition), The Williams and Wilkins Co., Baltimore, 1966.

APPENDIX I

MEAD MICRO-ANALYZER LENS AND FOCUS SELECTION

A. FOCUS CRITERION

In order to establish the scanning conditions for the granularity analysis, test scans were made on a single piece of type M film which was processed at MSFC in an automatic film processor. As part of the test two lens sets were used, specifically U1/L1 and U3/L3, where U1 is a Bausch and Lomb (B&L) 40 mm focal length; .08 numerical aperture lens; L1 is a B&L 48 mm, .08 lens; U3 is a B&L 215 mm, .25 lens; and L3 is a B&L 215 mm, .20 lens. The U3/L3 combination provided a depth of focus less than the film thickness while U1/L1 provided a depth of focus on the order of the film thickness. Both lens sets were employed in making several scans of a specific area on the film. Each scan was performed under various focusing conditions consisting of:

- Focus on lower emulsion
- Focus on upper emulsion
- Focus midway between emulsions
- Focus for maximum response

The criterion used to evaluate the optics and focusing techniques was the RMS granularity determined from scanning the control radiograph. The optics and focusing technique which yielded the maximum RMS granularity was assumed best for the analysis of the graininess and quantum mottle radiographs.

B. LENS COMBINATION SELECTION

For the short depth of focus lens combination U3/L3, the maximum RMS granularity was found to occur with the focus on the top emulsion layer. Lens combination U1/L1, with its greater depth of focus, was unable to distinguish between the two emulsion layers. However, the U1/L1 lens combination produced maximum granularity values equal to the maximum values achieved by the U3/L3 lens combination. Since the larger depth of focus of the U1/L1 lens provided a greater range of focus positions where maximum response could be obtained, it was selected for scanning of granularity and quantum mottle experiments.

To assure proper scanning of each radiograph the Micro-Analyzer should be re-focused for each radiograph. Because of the large number of radiographs which had to be scanned, a rapid method was required for accurate focusing. From several tests it was found that the optimum focus could be located by observing the analog output of the Micro-Analyzer on a paper chart recorder. This procedure was implemented in scanning the radiographs for the film grain and quantum mottle examinations.

APPENDIX II

RMS FILM GRANULARITY

A. MEAN AND VARIANCE OF A RANDOM VARIABLE

Given an experiment with a set S of outcomes, if we assign to each element α of S, according to some rule, the number X, we obtain the function $X(\alpha)$. The functional relationship between elements of S and the corresponding numbers X is called a random variable. One of the most important properties of a random variable X is its central tendency, called the expected value or mean of X, denoted by μ_X and defined by

$$\mu_X = E[X] = \int_{-\infty}^{\infty} xf(x)\,dx \tag{1}$$

where $f(x)$ is the probability density function (PDF) of the random variable X and the PDF at x represents the relative frequency of occurrence of the event α such that $X(\alpha) = x$. This definition of the mean is essentially equivalent to the concept of average given by

$$\lim_{N\to\infty} 1/N \sum_{i=1}^{N} X(\alpha_i)$$

Another important quality of a random variable X is the spread of values about the mean, called the variance of X, denoted by σ_X^2, and defined by

$$\sigma_X^2 = E[(X - \mu_X)^2] \tag{2}$$

The standard deviation of the random variable X, denoted by σ_X, is defined to be the square root of the variance:

$$\sigma_X = \sqrt{\sigma_X^2} \tag{3}$$

Given an experiment and the associated probability space S of outcomes, to every outcome α we can assign, according to some rule, a time or distance function denoted by $X(t,\alpha)$. Note that for a fixed α, $X(t,\alpha)$ is a single time or distance function. The ensemble or family of all these time or distance functions, for all elements α of S, is called a random process or stochastic process and is denoted by $X(t)$.

One of the most important properties of a random process is its central tendency, called the expected value or mean of the process. The mean of a process is generally dependent on time and is defined by

$$\mu_X(t) = E[X(t)] \tag{4}$$

Thus, the mean of the process at t is defined to be the mean of the random variable $X(t)$ defined by Eq. (1). The variance of the random process $X(t)$, denoted by $\sigma_X^2(t)$, is defined by

$$\sigma_X^2(t) = E\{[X(t) - \mu_X(t)]^2\} \tag{5}$$

Hence, the variance of the process at t is defined to be the variance of the random variable $X(t)$, defined by Eq. (2).

Another important property of a random process $X(t)$ is the correlation between values of the process at two different times. The autocorrelation of $X(t)$, denoted by $\rho(t_1, t_2)$ is defined by

$$\rho(t_1, t_2) = E\{[X(t_1) - \mu_X(t_1)][X(t_2) - \mu_X(t_2)]\} \tag{6}$$

A random process $X(t)$ is said to be "stationary" in the wide sense, or weakly stationary, if the mean of the process is constant and the autocorrelation depends only on time differences. This essentially means that the common first-order statistics of the random variables $X(t)$ are the same for all t. Thus, the mean and variance of a weakly stationary process $X(t)$ can be calculated using Equations (4) and (5), respectively, with only a single value of t.

In general, a stationary random process is said to be "ergodic" if all of its statistics can be determined from a single time record $X(t, \alpha_0)$. The mean and variance are often defined for a single time record by

$$\mu = \lim_{T\to\infty} 1/2T \int_{-T}^{T} X(t)dt$$

$$\sigma^2 = \lim_{T\to\infty} 1/2T \int_{-T}^{T} [X(t) - \mu]^2 dt$$

Although μ and σ^2 are actually random variables, it can be shown that

$$E[\mu] = \mu_X, \quad E[(\mu - \mu_X)] = 0, \quad E[\sigma^2] = \sigma_X^2, \quad E[(\sigma^2 - \sigma_X^2)] = 0$$

In the discrete case, μ and σ^2 are estimated from a single time record by

$$\hat{\mu} = 1/N \sum_{i=1}^{N} x_i \tag{7}$$

$$\hat{\sigma}^2 = (1/N-1) \sum_{i=1}^{N} [(x_i - \hat{\mu})^2] \tag{8}$$

where N is the number of samples in the record and $x_i = X(i\Delta t)$.

B. DATA SAMPLING

1. Independence of Sample Points:

In order to obtain the statistics of an ergodic random process, we must generally be satisfied with estimates of the statistics. These estimates are based on analyzing one or more discrete sample functions. For example, in order to estimate the mean of the process, we use the formula given by Equation (7). One of the most important properties of such an estimate is its accuracy, i.e., the numerical proximity of the estimated statistic to the actual statistic.

Generally the accuracy of an estimate improves with increasing sampling size. But particular caution must be exercized in utilizing this concept in the estimation of the first-order statistics (mean and variance). The accuracy of these statistics is a function of the number of statistically independent samples.

With respect to the grain noise process, statistical dependence of sample points arises in two ways. First, if the distance between two adjacent samples is smaller than the diameter of the scanning aperture, these samples will be dependent, since each of the densities arose partly from the same area on the film sample. Second, if the distance between two adjacent samples is smaller than the width of the grain noise autocorrelation function, these samples will be dependent, by definition of the autocorrelation function.

In determining the sample size for the desired accuracy of first-order statistical estimates, the two sources of statistical dependence noted above must be considered. For example, if N independent samples are required and the sampling interval is half the aperture diameter, approximately $2N$ such samples must be taken. Further, if the sampling interval is one-fifth the width of the autocorrelation function, at least $5N$ such samples must be taken.

2. Sampling Distributions:

If we consider a discrete sample function (time series) from an ergodic random process, we may look upon this sample of size N as observations of N random

variables. Moreover, any quantity computed from these sample values is also a random variable. For example, the estimate of the mean, given by Equation (7), is a random variable, since this estimate represents the sum of N random variables. The probability distribution of a sample statistic such as the sample mean is called a sampling distribution.

A number of sampling distributions naturally arise in practice. One of these is the well-known normal (Gaussian) distribution. Another is the Chi-Square distribution with n degrees of freedom, χ^2_n, defined as the sum of the squares of $n+1$ independent random variables, where each random variable has zero mean and unit variance. Another common sampling distribution is the Student t distribution with n degrees of freedom, t_n, defined by

$$t_n = Z/\sqrt{Y/n}$$

where Z and Y are independent random variables such that Y has a χ^2_n distribution and Z is normally distributed with zero mean and unit variance.

3. Sampling For the Mean:

Given the grain noise sample $X = \{x_1, x_2, \ldots, x_N\}$, we can obtain estimates of the mean and of the variance, $\hat{\mu}_X$ and $\hat{\sigma}^2_X$, by equations (7) and (8). Let us define

$$t_n = (\hat{\mu}_X - \mu_X)\sqrt{N}/\hat{\sigma}_X$$

where μ_X is the actual mean of the grain noise process. Since $\hat{\mu}_X$ and $\hat{\sigma}_X$ are random variables, t_n is also a random variable. Further, drawing on the Central Limit Theorem, $\hat{\mu}_X$ has a normal distribution; hence, t_n has a Student t distribution. The probability density function of t_n as a function of n and α, has been tabulated in such a way that

$$\text{prob}\ \{St_{n;1-\alpha/2} \leq t_n \leq St_{n;\alpha/2}\} = 1 - \alpha \qquad (9)$$

In Eq. (9) prob denotes probability of occurrence and St denotes the tabulated Student t distribution. The interval denoted in the braces of equation (9) is called the $(1-\alpha)$ x 100% confidence interval on t_n, since the probability that t_n lies in this interval is $1-\alpha$.

Since the probability density function of the Student t distribution is symmetric, we may denote the $(1-\alpha)$ x 100% confidence interval by

$$-k(n,\alpha) \leq t_n \leq k(n,\alpha) \tag{10}$$

where $k(n,\alpha)=St_{n;1-\alpha/2}=St_{n;\alpha/2}$. Manipulating the inequalities in (10), we obtain

$$-k(n,\alpha) \leq \frac{(\hat{\mu}_X - \mu_X)\sqrt{N}}{\hat{\sigma}_X} \leq k(n,\alpha)$$

$$\hat{\mu}_X - \frac{k(n,\alpha)\hat{\sigma}_X}{\sqrt{N}} \leq \mu_X \leq \hat{\mu}_X + \frac{k(n,\alpha)\hat{\sigma}_X}{\sqrt{N}} \tag{11}$$

Further, if we assume n (and hence N) is large, $k(n,\alpha)$ becomes a function of α only; so we may write (11) as

$$\hat{\mu}_X - \frac{k(\alpha)\hat{\sigma}_X}{\sqrt{N}} \leq \mu_X \leq \hat{\mu}_X + \frac{k(\alpha)\hat{\sigma}_X}{\sqrt{N}} \tag{12}$$

The inequality in (12) means that the probability is $1-\alpha$ that the true mean will be contained in the interval

$$\hat{\mu}_X \pm \frac{k(\alpha)\hat{\sigma}_X}{\sqrt{N}}$$

The computation required to determine the sample size N necessary to give a reasonable confidence interval for the mean can now be illustrated. For this purpose we will assume that $\hat{\sigma}_X = \sigma_X$ and that we seek an interval of length 0.01, centered at $\hat{\mu}_X$, such that this interval will contain μ_X at least 90% of the time. Thus, N satisfies the inequality

$$\frac{k(0.1)\sigma_X}{\sqrt{N}} \leq 0.005 \tag{13}$$

Solving (13) for N , we obtain

$$N \geq (1.645)^2 \sigma_X^2 / 0.005^2$$

where $k(0.1)=1.645$. For example, with a grain noise process where $\sigma_X=0.05$ at μ_X , $N \geq 271$ is required for a 90% confidence interval of 0.01 about $\hat{\mu}_X$.

4. Sampling for the Standard Deviation:

Let us define the parameter χ_n^2 by

$$\chi_n^2 = n\hat{\sigma}_X^2 / \sigma_X^2$$

where again $n=N-1$. Note that χ_n^2 has a Chi-Square distribution with n degrees of freedom. It can be shown that the parameter $\sqrt{2\chi_n^2}$ tends to a normal distribution for $n > 30$ with mean $\sqrt{2n-1}$ and unit variance. Thus, the variable G_n , defined by

$$G_n = \sqrt{\frac{2n\hat{\sigma}_X^2}{\sigma_X^2}} - \sqrt{2n-1}$$

has a normal sampling distribution with zero mean and unit variance. Thus, utilizing the tabulated values of the normal probability density function, we may say that

$$\text{prob}\{-k(\alpha) \leq G_n \leq k(\alpha)\} = 1 - \alpha \tag{14}$$

where

$$1/\sqrt{2\pi} \int_{-k(\alpha/2)}^{k(\alpha/2)} \exp(-t^2/2)\,dt = 1 - \alpha$$

Thus, the interval denoted in (14) represents the $(1-\alpha)$ x 100% confidence interval on G_n . Rearranging the description of this interval we obtain

$$-k(\alpha) \leq \frac{\sqrt{2n}\,\hat{\sigma}_X}{\sigma_X} - \sqrt{2n-1} \leq k(\alpha)$$

$$\frac{\sqrt{2n-1} - k(\alpha)}{\sqrt{2n}} \leq \frac{\hat{\sigma}_X}{\sigma_X} \leq \frac{\sqrt{2n-1} + k(\alpha)}{\sqrt{2n}} \tag{15}$$

The computation required to determine the sample size N necessary to give a reasonable confidence interval for the standard deviation can now be illustrated. As before, we let $\sigma_X=0.05$. We further assume that n is so large that $\sqrt{2n-1} \doteq \sqrt{2n}$. Lastly, we assume that it is desired to have a confidence interval about $\hat{\sigma}_X$ such that σ_X will be within 3% of $\hat{\sigma}_X$ 90% of the time. Hence the value of N (or n) required satisfies the inequality

$$0.97 \leq \frac{\sqrt{2n} - k(0.1)}{\sqrt{2n}}$$

$$0.97 \leq \frac{\sqrt{2n} - 1.645}{\sqrt{2n}}$$

$$0.97\sqrt{2n} \leq \sqrt{2n} - 1.645$$

$$1.645 \leq 0.03\sqrt{2n}$$

$$\sqrt{2n} \geq 55$$

$$2n \geq 3025$$

$$n \geq 1513$$

C. PRACTICAL CONSIDERATIONS

In the estimation of RMS film granularity, care must be taken in preparing the sample. The test film should be uniformly exposed and the processed film should be free of scratches, pinholes, and developer mottle. In practice, some deviations from such an ideal sample often occur. At Mead Technology Laboratories, any bias in granularity estimates induced by flaws in the film sample is minimized by the techniques employed by the analysis program (GRANSTAN). The theory behind the techniques used by GRANSTAN are detailed below.

1. Density Wedging:

One of the most frequently occurring defects in granularity samples is density wedging, whereby a variation in exposure across the sample causes a trend in density across the sample. Although careful exposure of the sample can minimize the magnitude of this wedging, some residual trends invariably occur. The technique employed by the GRANSTAN program minimizes the effects of such residual trends. This technique is based on estimating the variance of the grain noise process from the variance of the process defined by each independent adjacent difference (IAD) in the time record.

Let us denote a grain noise process by X, where we seek μ_X and σ_X^2. Suppose we are estimating μ_X and σ_X^2 from a time record $R=\{x_1,x_2,\ldots,x_N\}$, where each x_i is a realization of X; x_i and x_{i+1} statistically independent for each $i=1,2,\ldots,N-1$.

We assume that linear density wedging occurs, so that $\Delta d_i=k(i-1)$ is the bias at each i. Hence, the actual time record available is $S=\{x_i+\Delta d_i : i=1,2,\ldots,N\}$, where k is unknown and is the slope of the density variation across the sample.

Let us define a new process Y, where each realization of Y is the IAD of realizations of X. Hence, given the set of realizations S of X, the set of realizations T of Y is given by $T=\{D_i : i=1,2,\ldots,N/2\}$, where

$$D_i = (x_{2i} + \Delta d_{2i}) - (x_{2i-1} + \Delta d_{2i-1})$$

We will show that the variance of Y is precisely twice the variance of X, regardless of the magnitude of k.

According to Equation (1),

$$\mu_Y = E[Y]$$

Further,

$$D_i = x_{2i} - x_{2i-1} + \Delta d_{2i} - \Delta d_{2i-1} \tag{16}$$

and

$$\Delta d_{2i} - \Delta d_{2i-1} = k \tag{17}$$

Substituting (17) in (16) and noting that the expected value of each realization of X is μ_X, we have

$$\mu_Y = \mu_X - \mu_X + k = k \tag{18}$$

According to Equation (2),

$$\sigma_Y^2 = E[(Y - \mu_X)^2] \tag{19}$$

Drawing on Equation (16) and (17) and the result in (18), we have

$$\begin{aligned}
\sigma_Y^2 &= E[(x_{2i} - x_{2i-1} + k - k)^2] \\
&= E[x_{2i}^2 - 2x_{2i} \cdot x_{2i-1} + x_{2i-1}^2] \\
&= E[x_{2i}^2] - 2E[x_{2i} \cdot x_{2i-1}] + E[x_{2i-1}^2] \\
\sigma_Y^2 &= 2E[X^2] - 2\mu_X^2
\end{aligned} \tag{20}$$

where we have used the assumption that adjacent samples are statistically independent. Equation (20) can be manipulated in the following manner

$$\sigma_Y^2 = 2[E(X^2) - 2\mu_X^2 + \mu_X^2]$$

$$= 2[E(X^2) - 2E(X)\mu_X + \mu_X^2]$$

$$= 2E[(X - \mu_X)^2]$$

$$\sigma_Y^2 = 2\sigma_X^2 \qquad (21)$$

Thus, the GRANSTAN program actually estimates σ_X^2 by $\frac{1}{2}\sigma_Y^2$.

2. Random Flaws:

Random flaws, such as scratches and pinholes in the sample, while having little effect on the computed mean, can have significant effect on the computed variance. These flaws generally manifest themselves as density values which would otherwise not occur. Hence, the GRANSTAN program, if so directed, will discard typical densities in the sample. This editing is done on the basis of a histogram of the sample densities. If sampling was done in accordance with the guidelines prescribed above, the histogram of the sample will be more or less continuous. The GRANSTAN program searches for "holes" in the histogram on either side of the mode. Three adjacent densities which do not occur in the sample are used to identify the density range of the sample material. Densities which occur outside this range are discarded by the program before the sample statistics are estimated.

APPENDIX III

POWER SPECTRAL DENSITY

A. DEFINITIONS

The power spectrum of a stationary random process is defined as the Fourier transform of the autocovariance of the process. The power spectral density function for the process is defined as the power spectrum normalized by the variance of the process. In mathematical terms the autocovariance of a stationary random process $X(t)$ is:

$$g_{XX}(u) = E\left[(X(t) - \mu)\,(X(t+u) - \mu)\right] \tag{1}$$

where E denotes the expectation operator. The power spectrum of the process $X(t)$ is:

$$G(f) = \int_{-\infty}^{\infty} g_{XX}(u)\, e^{-j2\pi fu}\, du \tag{2}$$

There is also an inverse transform relation given by:

$$g_{XX}(u) = \int_{-\infty}^{\infty} G_{XX}(f)\, e^{j2\pi fu}\, df \tag{3}$$

Setting $u = o$ in (3) gives:

$$g_{XX}(o) = \sigma_X^2 = \int_{-\infty}^{\infty} G_{XX}(f)\, df$$

and shows how variance or 'power' of the $X(t)$ process is distributed over frequency.

The spectral density function is:

$$\frac{G_{XX}(f)}{\sigma_X^2} = \int_{-\infty}^{\infty} R_{XX}(u)\, e^{-j2\pi fu}\, du \tag{4}$$

where $R_{XX}(u)$ is the autocorrelation function of the random process $X(t)$. Since $G_{XX}(f)/\sigma_{XX}^2$ is non negative and $\int_{-\infty}^{\infty} G_{XX}(f)/\sigma_{XX}^2 = 1$ the term density function is appropriate.

In the previous discussion we considered an ideal case in which the stochastic process $X(t)$ was defined for all time $-\infty < t < \infty$. Suppose we only have available a record $x(t)$, $-\frac{T}{2} \leq t \leq T/2$, as one of many time series that might have been observed, that is, as a realization of the process $X(t)$. The sample power spectrum may be defined as the Fourier transform of the sample autocovariance function. The sample autocovariance is defined as:

$$C_{xx}(u) = \begin{cases} \frac{1}{T} \int_{0}^{T-|u|} (x(t)-x)\,(x(t+u)-x)\,dt & 0 \leq |u| \leq T \\ 0, & |u| > T \end{cases} \qquad (5)$$

The sample power spectrum is:

$$P_{xx}(f) = \int_{-T}^{T} C_{xx}(u)\, e^{-j2\pi fu}\, du, \quad -\infty \leq f \leq \infty \qquad (6)$$

The inverse Fourier transform of (6) may be written:

$$C_{xx}(u) = \int_{-\infty}^{\infty} P_{xx}(f)\, e^{j2\pi fu}\, df, \quad -T \leq u \leq T \qquad (7)$$

In discrete time, the sample spectrum is:

$$P_{xx}(f) = \Delta \sum_{k=-(K-1)}^{(K-1)} C_{xx}(k) e^{-j2\pi fk}, \quad -\tfrac{1}{2}\Delta \leq f < \tfrac{1}{2}\Delta \qquad (8)$$

The inverse transform of (8) is:

$$C_{xx}(u) = \int_{-1/2\Delta}^{1/2\Delta} P_{xx}(f) e^{j2\pi fu}\, df, \quad -n\Delta \leq u \leq n\Delta \qquad (9)$$

B. SAMPLE SPECTRUM STATISTICS

We have regarded the record $x(t)$, $-T/2 \leq t \leq T/2$ as a realization of a stochastic process $X(t)$. The variability in the sample record is characterized by rv's $X(t)$ for $-T/2 \leq t \leq T/2$. The sample spectrum $P_{xx}(f)$ can be regarded as a realization of the random variable $P_{XX}(f)$, just as the sample covariance function $C_{XX}(u)$ is normally regarded as a realization of the random variable

$C_{XX}(u)$. An examination of the variability in the sample power spectrum indicates some undesirable characteristics. Before discussing the nature of the problem, eq. (8) will be expressed in a different form. For the discrete case the sample spectrum is often defined as:

$$P_{xx}(f) = \frac{\Delta}{N}\left|\sum_{t=-N}^{N-1} X_t\, e^{-j2\pi\, ft\Delta}\right|^2$$

$$= \frac{\Delta}{N}\left\{\left(\sum_{t=-N}^{N-1} X_t \cos 2\pi\, ft\Delta\right)^2 + \left(\sum_{t=-N}^{N-1} X_t \sin 2\pi ft\right)^2\right.$$

$$1/2\Delta \leq f < 1/2\Delta \qquad (10)$$

where Δ is the sampling interval, $x(t)$ is a signal observed at times $t = -n\Delta\ ,\ -(n-1)\Delta\ ,\ \ldots,\ (n-1)\Delta$, and $N = 2n$.

It can be shown that eq's. (8) and (10) are equivalent. Eq. (10) is usually referred to as a sample spectrum estimator. For a purely random discrete process (discrete white noise) it can be shown that the variance of the sample spectrum estimator is independent of the number of observations N. However, the average of the sample spectrum is close to the theoretical value of the spectrum. These results follow from the sampling properties of the sample spectrum. To describe the sampling properties, we first consider the random variables associated with the real and imaginary Fourier components of a discrete purely normal process Z_t, $-n \leq t \leq n-1$. These are

$$R(f) = \sum_{t=-N}^{N-1} Z_t \cos 2\pi\, ft\Delta \qquad (11)$$

$$I(f) = \sum_{t=-N}^{N-1} Z_t \sin 2\pi\, ft\Delta\ ,\ -1/2\Delta \leq f < 1/2\Delta \qquad (12)$$

The sample spectrum estimator is then:

$$P_{ZZ}(f) = \Delta/N\left[R^2(f) + I^2(f)\right]\ ,\ -1/2\Delta \leq f < 1/2\Delta \qquad (13)$$

It can be shown that the following results hold:

1) The random variables

$$Y(f_k) = \frac{2P_{ZZ}(f_k)}{\Delta \sigma_Z^2} \quad , \quad k = \pm 1, \pm 2, \ldots, \pm(n-1) \qquad (14)$$

are distributed as χ_2^2 (chi square) random variables, where $f_k = k/N\Delta$.

2) When $f_k = 0$ or $f_k = -1/2\Delta$, the random variables

$$Y(f_k) = \frac{P_{ZZ}(f_k)}{\Delta \sigma_Z^2} \qquad (15)$$

are distributed as a χ_1^2 .

3) The random variables $Y(f_k)$ are mutually independent for $K = 0, \pm 1, \pm 2, \ldots, \pm(n-1), -n$.

It follows from 1) - 3) that:

$$E\left[P_{ZZ}(f_k)\right] = \sigma_Z^2 \Delta = G_{ZZ}(f_k) \qquad (16)$$

which means that the sample spectrum at the harmonic frequencies is an unbiased estimator of the spectrum for white noise. It also follows that:

$$\text{Var}\left[P_{ZZ}(f_k)\right] = \sigma_Z^4 \Delta^2 = G_{ZZ}^2(f_k) \qquad (17)$$

This shows that the variance of the estimator is a constant independent of the sample size. It should be noted that even if the Z_t process is not normal, the random variables $R(f)$ and $I(f)$ will be very nearly normal by the Central Limit Theorem. The distribution of $P_{ZZ}(f)$ will be close to a χ_2^2 regardless of the distribution of the Z_t process.

C. SMOOTHED SPECTRAL ESTIMATES

A general method has been developed for reducing the variance of the sample spectrum estimator by smoothing the spectral estimator. The smoothed spectral estimator is of the form:

$$\bar{P}_{XX}(f) = \int_{-\infty}^{\infty} w(u)\, C_{XX}(u)\, e^{-j2\pi fu}\, du \qquad (18)$$

The function $w(u)$ is referred to as a lag window and satisfies the conditions.

1) $w(o) = 1$
2) $w(u) = w(-u)$
3) $w(o) = o, |u| > T$

In practice condition 3) is replaced by:

4) $w(o) = o, \quad |u| \geq M, \quad M < T$

The Fourier transform $W(f)$ of the lag window $w(u)$ is referred to as a spectral window. Using a convolution property, Eq. (18) may be written as:

$$\bar{P}_{XX}(f) = \int_{-\infty}^{\infty} W(g) \; P_{XX}(f-g) \; dg$$

which is a smoothing of the sample spectrum $P_{XX}(f)$ by the spectral window $W(f)$. Analogous to the properties for the lag window, $W(f)$ satisfies the conditions.

1) $\int_{-\infty}^{\infty} W(f) \; df = 1,$
2) $W(f) = W(-f),$
3) $W(f)$ is a slit with base width of order $2/M$.

D. STATISTICS OF SMOOTHED SPECTRAL ESTIMATOR

We now examine the mean and variance of the smoothed spectral estimator. Taking expectations in Eq. 19 gives:

$$E\left[\bar{P}_{XX}(f)\right] = \int_{-\infty}^{\infty} W(g) \; E\left[P_{XX}(f-g)\right] \; dg$$

For large T, $E\left[P_{XX}(g)\right] \approx G_{XX}(g)$, so

$$E\left[\bar{P}_{XX}(f)\right] \approx \int_{-\infty}^{\infty} W(g) \; G_{XX}(f-g) \; dg = \bar{G}_{XX}(f) \qquad (20)$$

$\bar{G}_{XX}(f)$ is called the mean smoothed spectrum. The bias $B(f)$ associated with the smoothed spectral estimator is defined to be:

$$B(f) = E\left[\bar{P}_{XX}\right] - G_{XX} = \bar{G}_{XX}(f) - G_{XX}(f) \qquad (21)$$

It can be shown that to keep the bias small, M must be large. We will now show that this is contrary to the requirement to keep $\mathrm{Var}\left[\bar{P}_{XX}(f)\right]$ small. The variance of a smoothed spectral estimator can be approximated by:

$$\mathrm{Var}\left[\bar{P}_{XX}(f)\right] \approx \frac{G_{XX}^{2}(f)}{T} \int_{-\infty}^{\infty} W^{2}(g)\, dg \qquad (22)$$

or

$$\mathrm{Var}\left[\bar{P}_{XX}(f)\right] \approx \frac{G_{XX}^{2}(f)}{T} \int_{-\infty}^{\infty} W^{2}(u)\, du$$

For the Bartlett window this becomes:

$$\mathrm{Var}\left[\bar{P}_{XX}(f)\right] \approx \frac{G_{XX}^{2}(f)}{T} \left(\frac{2}{3}M\right) \qquad (23)$$

This shows that the variance of the smoothed spectral estimator can be reduced by making M small. However, reducing M increases the bias and causes more distortion of the theoretical spectrum. In order to partially resolve this conflict between bias and variance the level of discernible detail desired in the smoothed spectral estimate must be decided upon. In the next section of this report a method for choosing M is described based on the desired detail or resolution.

Previously, it was stated that the sample spectrum estimator $P_{XX}(f)$ is such that $2P_{XX}(f)/G_{XX}(f)$ is approximately distributed as χ^{2}_{2}. The corresponding result for the smoothed spectral estimator is that:

$$\gamma \bar{P}_{XX}(f)/G_{XX}(f)$$

is approximately distributed as χ^{2}_{γ} where $\gamma > 2$. Since $\gamma \bar{P}_{XX}(f)/G_{XX}(f)$ is distributed according to a χ^{2}_{γ}, it follows that:

$$P_r\left\{ \chi_\gamma \left(\frac{\alpha}{2}\right) < \frac{\gamma \bar{P}_{XX}(f)}{G(f)} \leq \chi_\nu \left(1-\frac{\alpha}{2}\right) \right\} = 1-\alpha \qquad (24)$$

where

$$P_r\left\{ \chi^2_\gamma \leq \chi_\gamma \left(\frac{\alpha}{2}\right) \right\} = \frac{\alpha}{2} \quad \text{and} \quad \nu = \frac{2T}{\int_{-\infty}^{\infty} w^2(u)\, du}$$

The interval between:

$$\frac{\nu \bar{P}_{XX}(f)}{\chi_\gamma (1-(\alpha/2))} \quad , \quad \frac{\nu \bar{P}_{XX}(f)}{\chi_\gamma (\alpha/2)} \qquad (25)$$

is a 100 $(1-\alpha)$ % confidence interval for $G_{XX}(f)$. It is convenient to plot spectra on a logarithmic scale, since then the confidence interval for the spectrum is simply represented by a constant interval about the spectral estimate. It follows from Eq. (25) that the confidence interval for log $G_{XX}(f)$ is:

$$\log \bar{P}_{xx}(f) + \log \frac{\nu}{\chi_\gamma (1-(\frac{\alpha}{2}))} \; , \; \log \bar{P}_{xx}(f) + \log \frac{\nu}{\chi_\gamma (\alpha/2)} \qquad (26)$$

E. BANDWIDTH

It was shown in eq. (22) that the term $S = \frac{1}{T}\int_{-\infty}^{\infty} W^2(u)\, du$ provides a measure of the reduction in variance of the estimator due to smoothing by a spectral window. In order to obtain a small variance it is necessary to make S small. For a given window W this can be done by making M small. Another useful characteristic of a window is its width. It can be shown that in order to obtain a good estimate of a peak in a spectrum, the 'width' of a spectral window must be of the same order as the width of the peak. The question arises as to what is meant by width of a spectral window since it is non zero for most f in the range $-\infty \leq f \leq \infty$. One way to define the width of a spectral window is to make use of the motion of width or bandwidth of a 'bandpass' spectral window. Considering the 'bandpass' spectral window:

$$W(f) = 1/h, \; -h/2 \leq f \leq h/2$$

we can see that the spectral window is rectangular in the frequency domain and has a unique width h, that is, its bandwidth b = h. Using Eq. (22), the variance of a smoothed spectral estimator based on this window is:

$$\text{Var}\left[\bar{P}_{XX}(f)\right] = G_{XX}^2(f)/Tb$$

Some authors have defined the bandwidth of the window as the width of the rectangular window that gives the same variance. That is,

$$\text{Var}\left[\bar{P}_{XX}(f)\right] \approx \frac{G_{XX}(f)}{T\,b} = \frac{G_{XX}^2(f)}{T}\int_{-\infty}^{\infty} w^2(u)\,du$$

which results in:

$$b = 1/\int_{-\infty}^{\infty} W^2(u)\,du$$

F. SPECTRAL ANALYSIS DESIGN

The basic requirements to be met in designing a spectral analysis calculation in advance of collecting the data are discussed below. The four basic requirements are:

1) The sampling interval Δ must be chosen small enough so that the spectral estimate can be obtained in the range of interest $o \leq f \leq f_o$. Based on the sampling theorem this requirement means that $\Delta \leq 1/2f_o$.

2) Aliasing must be avoided. This can be done in one of the following two ways.

   a) Choose Δ small enough so that the spectrum $G(f)$ is effectively zero for $f > 1/2\Delta$. This method requires initial knowledge of the spectrum and also if f_o is much less than the frequency beyond which $G(f)$ is effectively zero it may be necessary to collect data at a much finer sampling interval than is necessary to satisfy (1).

   b) The 2nd method is to filter the signal before sampling so that all frequencies above f_o are effectively removed.

3) This requirement is concerned with the resolution desired in the spectral estimate. If it is desired to "detect" detail of width or more in the spectrum, then the truncation point M should be chosen so that the bandwidth b is less than a. For the Tukey window this means that $b = 1.33/M \leq a$ or $M = L\Delta \geq 1.33/a$ or $L \geq 1.33/a\,\Delta$.

4) For finite records the variance of the estimator will influence the amount of fine detail in the spectral estimate. Peaks may be due to the variability of the spectral estimate. In order to tie the estimate down to a given stability, it is necessary to specify the number of degrees of freedom γ desired with each estimate. The record length necessary to obtain the specified value of γ is given by the formula:

$$T = \gamma/2a$$

or

$$N = \gamma/2a$$

where a was defined in (3). A confidence interval based on the chi-squared distribution can be determined for the given number of degrees of freedom. It should be noted that it may be necessary to process very long records or large amounts of data to obtain a narrow high confidence band (95%) about the spectral estimate.

APPENDIX IV
EDGE GRADIENT ANALYSIS

A. SYSTEM PERFORMANCE MEASURES

If an imaging system is linear, it can be characterized by its optical transfer function (OTF) defined by:

$$\text{OTF}(f) = \frac{\mathcal{F}\{\theta(x)\}(f)}{\mathcal{F}\{i(x)\}(f)} \qquad (1)$$

where f is spatial frequency;

$\mathcal{F}\{\ \}(f)$ denotes the Fourier transform operator defined by

$$\mathcal{F}\{\alpha(x)\}(f) = \int_{-\infty}^{\infty} \alpha(x) \exp(-2\pi i f x)\, dx$$

$i(x)$ represents an input function to the system (target);

$\theta(x)$ represents the corresponding output function of the system (image).

The OTF is generally a complex function. The system performance measure usually reported is the (normalized) modulation transfer function defined by:

$$\text{MTF}(f) = \frac{|\text{OTF}(f)|}{|\text{OTF}(o)|} \qquad (2)$$

where $|\ |$ denotes the absolute value function.

There are several items of interest in Equation (2). First, the MTF is scaled so that MTF(0) = 1. Hence, at some spatial frequency f_o, MTF (f_o) answers the following question:

> Given a sine-wave input to the system of the form $i(x) = a + b \sin(2\pi f_o x)$, i.e., with spatial frequency f_o and modulation b/a, by what factor will the modulation be reduced by the system?

Second, if the system is truly linear, Equation (2) is valid for any target function having frequency content. But if we are interested in the MTF out to a specific spatial frequency, the Fourier transform of the target should have positive magnitude at that frequency.

B. APPLICATION OF EDGES AS TARGETS

One of the most common target functions is the edge target, where $i(x)$ is the Heaviside function:

$$H(x) = \begin{cases} 0 & \text{for } x \leq 0 \\ 1 & \text{for } x > 0 \end{cases} \tag{3}$$

Equation (2) cannot be used directly for edge analysis, since the Heaviside function does not have a Fourier transform. In this case, we draw on the fundamental result of linear system theory, namely that $\theta(x)$ is the convolution of $i(x)$ with the system impulse reponse (spread function), $s(x)$. Equation (2) may be written as:

$$\text{MTF}(f) = \left| \frac{\mathcal{F}\{i(x) * s(x)\}(f)}{\mathcal{F}\{i(x)\}(f)} \right| \tag{4}$$

where $i(x)$ is some function possessing a Fourier transform and $*$ is the convolution operation defined by:

$$\alpha * \beta(x) = \int_{-\infty}^{\infty} \alpha(\mu)\, \beta(x - \mu)\, d\mu \tag{5}$$

Equation (4) may be written as:

$$\text{MTF}(f) = \left| \frac{\mathcal{F}\{i(x)\}(f)\, \mathcal{F}\{s(x)\}(f)}{\mathcal{F}\{i(x)\}(f)} \right|$$

$$\text{MTF}(f) = |\mathcal{F}\{s(x)\}(f)| \tag{6}$$

In the case of the edge target, $\theta(x)$ is the convolution of s with the heaviside function. Therefore,

$$\theta(x) = s(x) * H(x) \tag{7}$$

After some manipulations, Equation (7) may be written as:

$$\theta(x) = \int_{0}^{x} s(\mu)\, du \tag{8}$$

And, differentiating both members of Equation (8), the following is obtained:

And, differentiating both members of Equation (8), the following is obtained:

$$\theta'(x) = s(x) \tag{9}$$

Hence, edge gradient analysis involves the use of Equations (9) and (6); that is, differentiating the edge reponse to obtain the spread function, then Fourier transforming the spread function to obtain the MTF. The differentiation step involved in using these equations is generally avoided by the use of integration by parts:

$$\begin{aligned} \text{MTF}(f) &= \left| \mathcal{F}\{\theta'(x)\}(f) \right| \\ &= \left| \int_0^{\Delta} \theta'(x) \exp(-2\pi i f x)\, dx \right| \qquad (10) \\ &= \left| \theta(x) \exp(-2\pi i f x) \right|_0^{\Delta} + 2\pi i f \int_0^{\Delta} \theta(x) \exp(-2\pi i f x)\, dx \\ \text{MTF}(f) &= \left| \exp(-2\pi i f \Delta) + 2\pi i f \int_0^{\Delta} \theta(x) \exp(-2\pi i f x)\, dx \right| \end{aligned}$$

where the interval from 0 to Δ contains the edge response $\theta(x)$. Equation (10) is the fundamental equation of edge gradient analysis.